nature immunology

Article

https://doi.org/10.1038/s41590-023-01419-y

Phosphoinositide acyl chain saturation drives CD8$^+$ effector T cell signaling and function

Received: 3 May 2022

Accepted: 3 January 2023

Published online: 2 February 2023

Check for updates

Joy Edwards-Hicks[1,10], Petya Apostolova[1,2,10], Joerg M. Buescher[1], Hannes Maib[3], Michal A. Stanczak[1,2], Mauro Corrado[1], Ramon I. Klein Geltink[1], Maria Elena Maccari[4], Matteo Villa[1], Gustavo E. Carrizo[1,2], David E. Sanin[1,2], Francesc Baixauli[1], Beth Kelly[1,2], Jonathan D. Curtis[1,2], Fabian Haessler[1], Annette Patterson[1], Cameron S. Field[1], George Caputa[1], Ryan L. Kyle[1], Melanie Soballa[1], Minsun Cha[2], Harry Paul[2], Jacob Martin[2], Katarzyna M. Grzes[1,2], Lea Flachsmann[1], Michael Mitterer[1], Liang Zhao[2], Frances Winkler[5,6], David Ali Rafei-Shamsabadi[7], Frank Meiss[7], Bertram Bengsch[5,8], Robert Zeiser[8,9], Daniel J. Puleston[1,2], David O'Sullivan[1], Edward J. Pearce[1,2,6] & Erika L. Pearce[1,2] ✉

How lipidome changes support CD8$^+$ effector T (T_{eff}) cell differentiation is not well understood. Here we show that, although naive T cells are rich in polyunsaturated phosphoinositides (PIP_n with 3–4 double bonds), T_{eff} cells have unique PIP_n marked by saturated fatty acyl chains (0–2 double bonds). PIP_n are precursors for second messengers. Polyunsaturated phosphatidylinositol bisphosphate (PIP_2) exclusively supported signaling immediately upon T cell antigen receptor activation. In late T_{eff} cells, activity of phospholipase C-γ1, the enzyme that cleaves PIP_2 into downstream mediators, waned, and saturated PIP_n became essential for sustained signaling. Saturated PIP was more rapidly converted to PIP_2 with subsequent recruitment of phospholipase C-γ1, and loss of saturated PIP_n impaired T_{eff} cell fitness and function, even in cells with abundant polyunsaturated PIP_n. Glucose was the substrate for de novo PIP_n synthesis, and was rapidly utilized for saturated PIP_2 generation. Thus, separate PIP_n pools with distinct acyl chain compositions and metabolic dependencies drive important signaling events to initiate and then sustain effector function during CD8+ T cell differentiation.

Metabolic reprogramming during T cell activation is required to support the increased biosynthetic demands of CD8$^+$ T_{eff} cell proliferation, effector function and epigenetic remodeling needed to enforce differentiation[1,2]. Metabolites also directly modulate the activity of signaling pathways (for example, amino acids regulate mammalian target of rapamycin (mTOR), ATP/AMP regulates AMP-activated protein kinase (AMPK), phosphoenolpyruvate regulates sarco/endoplasmic reticulum Ca^{2+}-ATPase (SERCA))[3], tying T cell signaling to metabolite acquisition. While changes in polar metabolites during CD8$^+$ T cell activation have been studied[4–7], less is known about lipid metabolism and how polar metabolites impact lipid signaling.

Phosphatidylinositol (PI) is one of eight phospholipids of the phosphoinositide (PIP_n) family that differ in their inositol headgroup that can be unphosphorylated (PI), or phosphorylated at one or more

A full list of affiliations appears at the end of the paper. ✉e-mail: epearce6@jhmi.edu

specific sites (PI(3)P, PI(4)P, PI(5)P, PI(4,5)P_2, PI(3,4)P_2, PI(3,5)P_2, PI(3,4,5)P_3). Mammalian cells have PIP_n with a dominant acyl chain composition (38:4), in contrast to most other phospholipids that display a range of chain lengths and saturation[8]. In 38:4 PIP_n, the 38 denotes the numbers of carbons in the acyl chains, and 4 denotes the double bonds, which decrease with increasing saturation. In mammalian cells, 19 kinases and 29 phosphatases dynamically interconvert family members to regulate PIP_n signaling[9]. The introduction of 'new' PIP_n, which increases the net PIP_n pool, occurs through de novo synthesis of unphosphorylated PI. PIP_2 and PIP_3 represent less than 1% of membrane phospholipids, but are essential for many cellular processes, including cytoskeletal organization, phagocytosis, endocytosis and exocytosis[10]. T cell antigen receptor (TCR) ligation initiates rapid PIP_n interconversion (phosphorylation and dephosphorylation) and salvage, marked by phospholipase C (PLC)-mediated PIP_2 hydrolysis and PIP_2 phosphorylation to PIP_3 by phosphoinositide 3-kinase (PI3K)[11]. Phospholipase C-γ1 (PLCγ1) is the predominant isoform in T cells and its activity is regulated by the proximal signaling complex that is formed upon TCR ligation[10]. PIP_2 hydrolysis generates the membrane lipid diacylglycerol (DAG) and soluble inositol triphosphate (IP_3)[12]. DAG recruits and activates several proteins, including Ras guanyl nucleotide-releasing proteins, which in turn activate Ras, the kinase Raf and the downstream MEK1/2–ERK1/2 cascade that promotes gene expression important for T_{eff} cell activation and survival[13]. IP_3 binds endomplasmic reticulum (ER) membrane receptors to release stored Ca^{2+} into the cytosol, initiate store-operated calcium entry, activate downstream target enzymes and transcription factors and regulate remodeling of the filamentous actin (F-actin) cytoskeleton required for T cell migration[14,15].

It has been a longstanding question whether discrete PIP_2 pools are essential for specific cellular effects[16–18]. Here we show that T_{eff} cells are equipped with a distinct PIP_2 pool with saturated acyl chains (we refer to PIP_n with 0–2 double bonds as saturated) that differs from the polyunsaturated PIP_2 pool of unactivated T cells (we refer to PIP_n with 3–4 double bonds as polyunsaturated). We found that specific T cell programs utilize these different PIP_n to drive signaling events. Saturated PIP_n mediate T_{eff} cell signaling, while polyunsaturated PIP_n exclusively mediate signaling early after T cell activation. Our data also show that glucose is the major substrate of T_{eff} cell de novo PIP_n synthesis, implicating PIP_n as an important link between extracellular glucose availability, glycolytic metabolism and T_{eff} cell signaling and function.

Results

$CD8^+$ effector T cells synthesize PIP_n with saturated acyl chains

We stimulated mouse $CD8^+$ T cells with anti-CD3/CD28 plus interleukin (IL)-2 for 3 d in vitro and compared them to unstimulated $CD8^+$ T cells cultured in IL-7 (Fig. 1a). Using liquid chromatography coupled with triple quadrupole tandem mass spectrometry (LC–QqQ–MS/MS), we detected over 300 lipids from 18 lipid subclasses in stimulated $CD8^+$ T cells (Extended Data Fig. 1a) with a general increase in lipid content (Extended Data Fig. 1b). To potentially identify lipids with important biological functions beyond building biomass, we performed quantile normalization of lipid content before comparing changes in individual lipid species between unstimulated and stimulated $CD8^+$ T cells (Extended Data Fig. 1b). We identified 11 PI species that increased in T_{eff} cells (Fig. 1b) relative to unstimulated T cells—where PI 38:4 was the most abundant (Fig. 1c). PI 38:4 is the predominant PI species (>70%) in most mammalian cells[8], and when corrected for cell size changes, it did not increase with stimulation (Fig. 1c). However, in T_{eff} cells, PI species with 0–2 double bonds increased (Fig. 1d), shifting the overall PI composition toward saturated (Fig. 1e). Enhanced saturated PI synthesis in T_{eff} cells increased total PI relative to other lipids (Extended Data Fig. 1c) and increased the PI concentration per cell (Fig. 1f). PIP_n signaling is regulated by de novo PI synthesis that introduces new PIP_n, and by PIP_n phosphorylation or dephosphorylation of the inositol headgroup (Fig. 1g). Although we could not distinguish between PI(4,5)P_2, PI(3,4)P_2 and PI(3,5)P_2, we found that T_{eff} cells had an increase in total PIP_2 species with 0–2 double bonds, which shifted the overall PIP_2 composition toward saturated (Fig. 1h). Total polyunsaturated PIP_2 species (with ≥3 double bonds) did not change between unstimulated T cells and T_{eff} cells (Fig. 1h). Total PI(3,4,5)P_3 (PIP_3) species with 0–2 double bonds increased in T_{eff} cells and shifted the PIP_3 composition toward saturated (Fig. 1i); however, in contrast to PI and PIP_2, the total amount of PIP_3 decreased in T_{eff} cells, as described for T cells 20 h after activation[19].

To confirm increased PI saturation in physiologically activated antigen-specific mouse $CD8^+$ T cells, we adoptively transferred OVA-specific (OT-I) $CD8^+$ T cells into recipient mice followed by infection with *Listeria monocytogenes* expressing OVA (LmOVA, Fig. 1j). $CD8^+$ T cells from LmOVA-infected mice compared to uninfected OT-I mice did not have increased PI per cell (Fig. 1k); however, their overall PI composition shifted toward saturated (Fig. 1l), and the total saturated PI was elevated (Fig. 1m). We made a similar observation when we subcutaneously inoculated mice with B16-F10 melanoma and isolated $CD8^+$ T cells either from the tumor or spleen when the tumors reached 7 mm in diameter (Fig. 1n). Compared to splenic $CD8^+$ T cells, tumor-infiltrating lymphocytes (TILs) had an increased concentration of PI (Fig. 1o) with a shift toward saturated species (Fig. 1p,q). Thus, PIP_n species with saturated acyl chains accumulate in mouse $CD8^+$ T_{eff} cells in vitro and in vivo.

We next stimulated human $CD8^+$ T cells with anti-CD3/CD28 and IL-2 for 5 d in vitro and compared them to newly isolated unstimulated $CD8^+$ T cells (Extended Data Fig. 1d). We observed increased saturated PI, and like mouse T cells, PI 38:4 was the predominant PI in human unstimulated T cells and it was not specifically enriched after activation (Extended Data

Fig. 1 | $CD8^+$ effector T cells synthesize PIP_n with saturated acyl chains. **a**, Experimental scheme. WT $CD8^+$ T cells were stimulated (Stim) with anti-CD3, anti-CD28 and IL-2, or cultured with IL-7 (Unstim), for three d. **b**,**c**, Relative and absolute lipid intensities, respectively. $n = 9$ biologically independent samples from three independent experiments; ordinary one-way analysis of variance ANOVA (**b**) or two-way ANOVA (**c**) corrected for multiple comparisons (Sidak test). **d**, Relative intensity (log_2 fold change) of saturated PI normalized to unstimulated $n = 9$ biologically independent samples from three independent experiments; one-sample *t*-test. **e**, Percentage PI saturation. $n = 9$ biologically independent samples from three independent experiments; unpaired two-tailed *t*-test comparing saturated PIs. **f**, Total PI concentration (nmol/cell). $n = 9$ biologically independent samples from three independent experiments; unpaired two-tailed *t*-test. **g**, PIP_n synthesis and interconversion scheme. **h**, Total (left) and percentage (right) PIP_2 saturation. $n = 3$ biologically independent samples, representative of two independent experiments; unpaired two-tailed *t*-test comparing the percentage of saturated PIP_2; total polyunsaturated PIP_2 = not significant. **i**, Total (left) and percentage (right) PIP_3 saturation. $n = 3$ biologically independent samples, representative of two independent experiments; unpaired two-tailed *t*-test comparing the total or percentage saturated PIP_3; total polyunsaturated PIP_3 = $P < 0.001$. **j**, Experimental scheme. OT-I $CD45.2^+$ $CD8^+$ T cells (OT-I) were adoptively transferred into $CD45.1^+$ C57BL/6 mice (1×10^6 cells per mouse). One day later mice were infected intravenously (i.v.) with LmOVA. Four d later, WT $CD45.2^+/CD8^+$ T cells were isolated from infected (Lm) or uninfected (CTRL) mice. **k**–**m** Total PI concentration (nmol/cell), percentage PI saturation and relative intensity (log_2 fold change) of saturated PI normalized to CTRL. $n = 3$ Ctrl and 12 Lm biologically independent samples; unpaired two-tailed *t*-test: total PI, percentage saturated PI; one-sample *t*-test: relative saturated PI. **n**, Experimental scheme. Sex-matched C57BL/6 mice were injected in the right flank with 1×10^6 B16-F10-OVA cells. Tumor growth was measured up to an average of 7 mm in diameter, then $CD8^+$ T cells were isolated from the spleen (SP) or tumor (TIL). **o**–**q**, Total PI concentration (nmol/cell), percentage PI saturation and relative intensity (log_2 fold change) of saturated PI normalized to SP. $n = 5$ biologically independent samples; unpaired two-tailed *t*-test: total PI, percentage saturated PI; one-sample *t*-test: relative saturated PI. Error bars show the s.e.m. a.u., arbitrary units.

https://doi.org/10.1038/s41590-023-01419-y

Fig. 1e,f). PI with 0–2 double bonds increased (Extended Data Fig. 1g), shifting the overall PI composition toward saturated (Extended Data Fig. 1h). Total PI increased relative to other lipids (Extended Data Fig. 1i), aligning with an increased PI concentration (Extended Data Fig. 1j). Changes in the amount and degree of PIP_2 and PIP_3 saturation in human T_{eff} cells also matched the observations in mouse T_{eff} cells (Extended Data Fig. 1k,l). To investigate in vivo, we compared circulating $CD8^+$ T cells from the blood of healthy donors or participants with acute Epstein–Barr virus (EBV) infection (Extended Data Fig. 1m). $CD8^+$ T cells in participants with acute EBV infection extensively proliferated (Extended Data Fig. 1n)[20], and their $CD8^+$ T cells had elevated PI species with 0–2 double bonds (Extended Data Fig. 1o) that shifted the PI composition toward saturated (Extended Data Fig. 1p), with a similar PI concentration per cell (Extended Data Fig. 1q). Thus, PIP_n species with saturated acyl chains accumulate in in vitro-generated and in vivo-generated mouse and human $CD8^+$ T_{eff} cells and results in saturated PIP_2 accumulation.

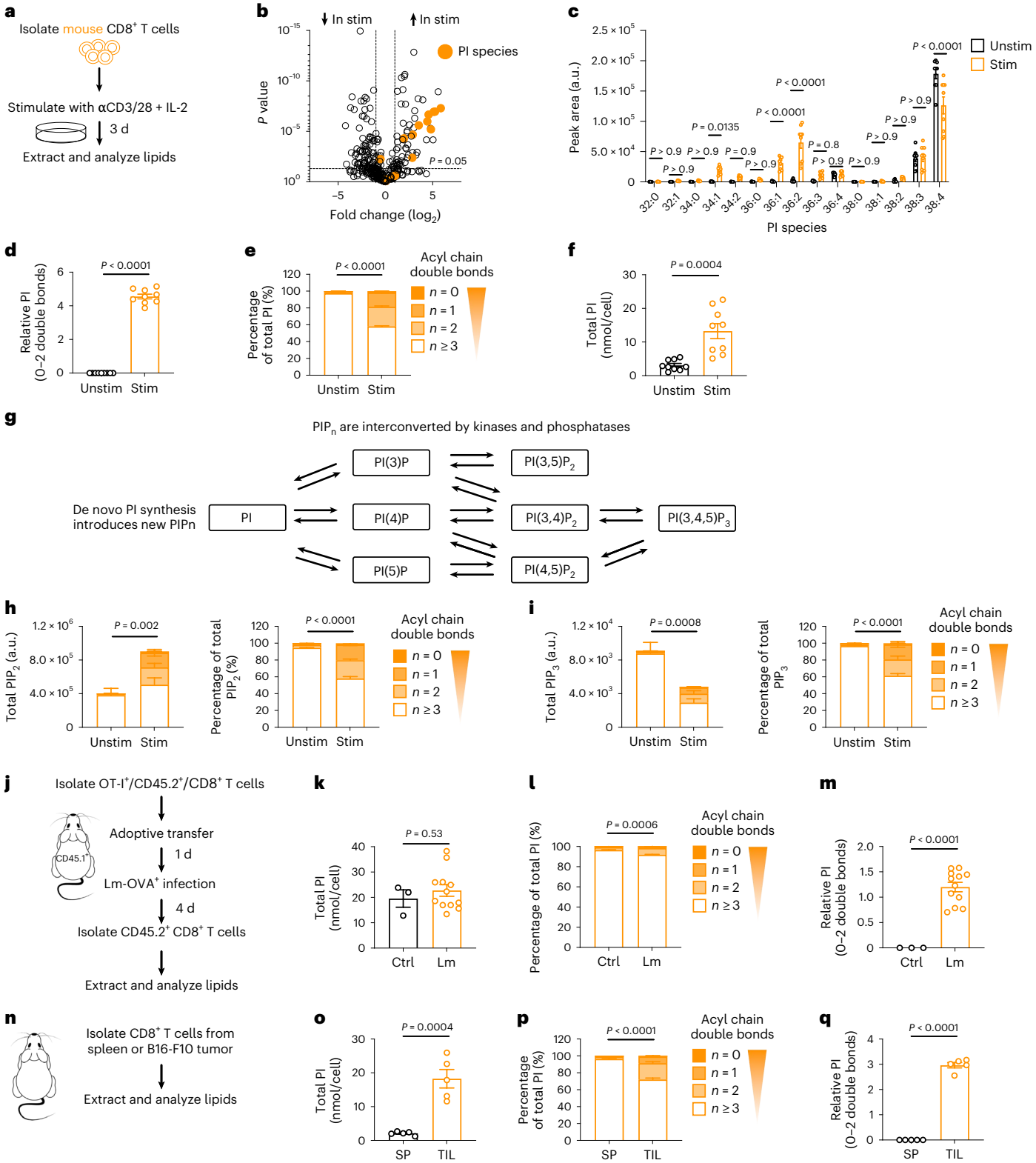

https://doi.org/10.1038/s41590-023-01419-y

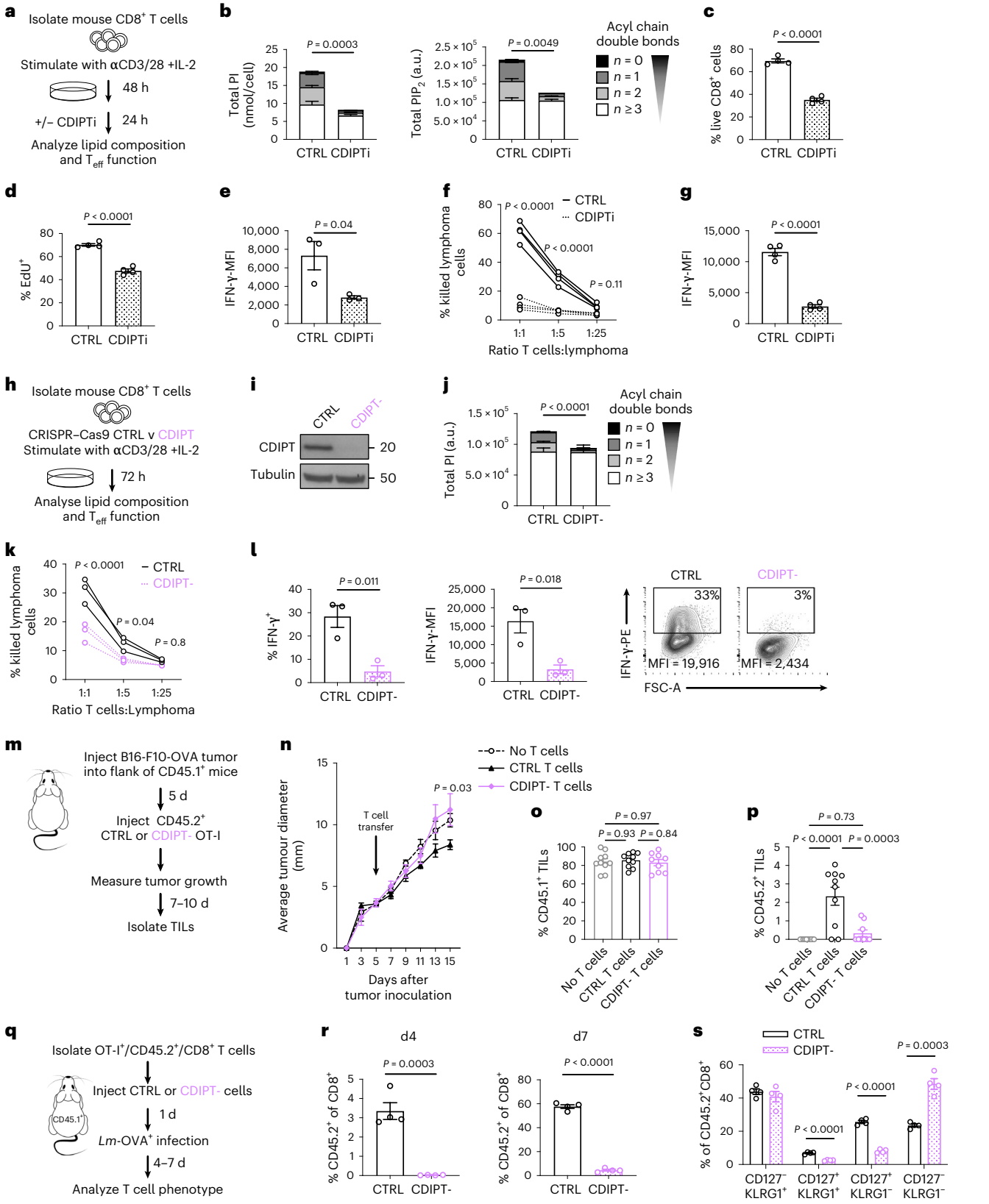

De novo PIP_n synthesis is essential for effector T cell fitness and function

In the final step of de novo PI synthesis, CDP-diacylglycerol-inositol 3-phosphatidyltransferase (CDIPT, Extended Data Fig. 2a)[8] transfers free inositol to CDP-diacylglycerol (CDP-DAG). We cultured cells for the last 24 h of activation with vehicle (CTRL) or inostamycin, a CDIPT inhibitor (CDIPTi)[21] (Fig. 2a). CDIPTi treatment depleted saturated PI species, but only partially decreased polyunsaturated PI (Fig. 2b). This indicated that saturated PI was mainly synthesized through the de novo pathway, while polyunsaturated PI could also be synthesized through remodeling lysophosphatidylinositol (LPI). Consistently, LPI decreased following CDIPTi treatment (Extended Data Fig. 2a,b). We

Fig. 2 | De novo PIP_n synthesis is essential for effector T cell fitness and cytotoxic function. **a**, Experimental scheme. **b**, PI (left) or PIP_2 (right) acyl chain saturation. $n = 4$ biologically independent samples, representative of three independent experiments for PI and one experiment for PIP_2; unpaired two-tailed *t*-test comparing saturated PI or PIP_2. **c**, Percentage of live, $CD8^+$ T cells gated on Live/Dead-blue$^-$ and CD8-FITC$^+$. **d**, Incorporation of EdU into newly synthesized DNA. **e**, Intracellular expression of IFN-γ quantified by flow cytometry. Cells were gated on Live/Dead-IR$^-$, CD8-BV421$^+$. In **c**–**d**, n=4 and in **e**, $n = 3$ biologically independent samples, representative of three independent experiments; unpaired two-tailed *t*-test. **f**,**g**, OT-I were activated by SIINFEKL peptide with IL-2 for 2 d, treated with CTRL or CDIPTi (plus IL-2), then co-cultured at the indicated ratio with Cell Trace Violet (CTV)-stained EL4-OVA for eight h. **f**, Percentage killing was determined by CTV$^+$, Live/Dead-IR$^+$ cells. **g**, Cells co-cultured at a 1:1 ratio in the presence of brefeldin A. IFN-γ expression in Live/Dead-IR$^-$ and CD8-APC$^+$ cells. $n = 4$ biologically independent samples; two-way ANOVA corrected for multiple comparisons (Sidak test) (**f**) or unpaired two-tailed *t*-test (**g**). **h**, Experimental scheme. **i**, Protein expression of CDIPT. $n = 3$ biologically independent samples pooled into a single lane. **j**, PI saturation. $n = 4$ biologically independent samples; unpaired two-tailed *t*-test on saturated PI. **k**,**l**, EL4-OVA co-culture as in **f** and **g**. $n = 3$ biologically independent samples; two-way ANOVA corrected for multiple comparisons (Sidak test) (**k**) or unpaired two-tailed *t*-test (**l**). **m**, Experimental scheme. **n**, Tumor growth. $n = 5$ biologically independent samples; two-way ANOVA corrected for multiple comparisons (Dunnett test) comparing no T cell transfer, to transfer of CTRL or CDIPT$^-$ T cells at each time point. **o**,**p**, Tumors were stained for congenic markers. Cells were gated on LD-Aqua$^-$, CD8-APC-Cy7$^+$ and the percentage of CD45.1-PE-Cy7$^+$ (**o**) or CD45.2-FITC$^+$ (**p**) cells is shown. $n = 10$ represents no T cell transfer and CTRL and $n = 9$ represents CDIPT$^-$ biologically independent samples; one-way ANOVA corrected for multiple comparisons (Tukey test). **q**, Experimental scheme. **r**,**s**, At four and seven d after infection, blood samples from infected mice were analyzed by flow cytometry for the expression of CD8, CD45.1, CD45.2, CD127 and KLRG1. $n = 4$ biologically independent samples per group; unpaired two-tailed *t*-test. All error bars show the s.e.m. MFI, mean fluorescence intensity.

observed a marked decrease in saturated PIP_2, while the polyunsaturated PIP_2 pool was unchanged (Fig. 2b). This demonstrated that CDIPT inhibition selectively targeted saturated PIP_2 synthesis, and indicated preference for phosphorylation of saturated PI, despite an abundance of polyunsaturated PI (Fig. 2b).

$CD8^+$ T cell viability (Fig. 2c and Extended Data Fig. 2c), proliferation (Fig. 2d and Extended Data Fig. 2d) and interferon (IFN)-γ production (Fig. 2e) decreased after CDIPTi treatment. We tested whether restoring PI composition could rescue CDIPT inhibition by treating cells with bovine serum albumin (BSA)-conjugated Soy PI, which comprises only saturated PI species (Extended Data Fig. 2e). Soy PI treatment shifted the intracellular PI pool toward saturated (Extended Data Fig. 2f), and partially restored the reduced IFN-γ expression after CDIPTi treatment (Extended Data Fig. 2g). Substitution with polyunsaturated PI 38:4 shifted the total PI pool toward polyunsaturated (Extended Data Fig. 2h), but it did not restore IFN-γ production upon CDIPT inhibition (Extended Data Fig. 2i). CDIPTi-treated OT-I $CD8^+$ T cells had a reduced ability to kill OVA-expressing EL4 tumor cells and decreased IFN-γ production when co-cultured with tumor cells (Fig. 2f,g). CDIPT inhibition also resulted in lower viability, EdU incorporation and IFN-γ production when treatment was started on day four or six of culture (Extended Data Fig. 2j). Of note, the effects of CDIPTi treatment were reversible as cells recovered viability, proliferation and cytokine production after drug withdrawal (Extended Data Fig. 2k). These data indicate that de novo PI synthesis is required to synthesize saturated PIP_n, which are needed for T_{eff} cell fitness and function.

To reinforce our CDIPTi findings, we used CRISPR–Cas9 to delete CDIPT (CDIPT$^-$) in $CD8^+$ T cells before activation (Fig. 2h,i). We observed a specific decrease of saturated PI in CDIPT$^-$ cells compared to CTRL (Fig. 2j), which confirmed that $CD8^+$ T_{eff} cells rely on CDIPT-dependent de novo PI synthesis to synthesize saturated PI. Importantly, whether CDIPT was pharmacologically inhibited, or genetically deleted, activated T cells maintained substantial and unperturbed pools of polyunsaturated PI (Fig. 2b,j). CDIPT$^-$ cells displayed impaired EL4-OVA cell killing and IFN-γ expression (Fig. 2k,l). To assess in vivo, we injected B16-F10-OVA melanoma cells into the flanks of wild-type (WT) mice, then adoptively transferred CTRL OT-I cells, CDIPT$^-$ OT-I cells or no T cells five d after tumor inoculation (Fig. 2m). We observed reduced tumor control in the CDIPT$^-$ T cell group relative to the CTRL group, similarly to the no T cell transfer group (Fig. 2n). CDIPT$^-$ OT-I cells failed to persist in vivo compared to CTRL OT-I cells, highlighted by decreased percentages of tumor-infiltrating donor-derived CD45.2$^+$ cells (Fig. 2o,p). We further tested CDIPT$^-$ T cell fitness by injecting CTRL and CDIPT$^-$ OT-I cells in LmOVA-infected mice (Fig. 2q). Expansion of CDIPT$^-$ donor T cells was almost completely abolished four and seven d after infection (Fig. 2r). Among the remaining donor T cells, we observed fewer memory precursor effector cells (CD127$^+$ KLRG1$^-$, Fig. 2s)[22]. Together, these results indicate that saturated PIP_n synthesis via CDIPT is required for $CD8^+$ T_{eff} cell fitness and function during cancer and infection.

Saturated PIP_n are dispensable for early $CD8^+$ T cell activation

PIP_n are critical signaling mediators downstream of the TCR[23]. Inositol headgroup phosphorylation transduces signals by activating alternate signaling networks, which in turn control cell differentiation[24]. Given our findings that PIP_n acyl chain saturation impacts T_{eff} cell fitness and function, we next asked whether saturated PIP_n are important early during T cell activation. The PIP_2 pool increased in the first hours

Fig. 3 | Saturated PIP_n are dispensable for early $CD8^+$ T cell activation. **a**–**c**, WT $CD8^+$ T cells were stimulated with anti-CD3, anti-CD28 and IL-2 for 6 h. Intracellular lipids were analyzed by LC–QqQ–MS/MS or liquid chromatography quadrupole time-of-flight mass spectrometry (LC–QTOF–MS/MS). **a**, Total PIP_2 at indicated time points after activation. $n = 5$ biologically independent samples; unpaired two-tailed *t*-test comparing total PIP_2. **b**, Increase in PIP_2 species with 0–2 versus ≥3 double bonds between zero h and six h after activation. $n = 5$ biologically independent samples; unpaired two-tailed *t*-test. **c**, Total PI at indicated time points after activation. $n = 5$ biologically independent samples; unpaired two-tailed *t*-test comparing total PI. **d**–**h**, WT $CD8^+$ T cells were isolated from C57BL/6 mice, then CRISPR–Cas9 technology was utilized to delete CDIPT (CDIPT$^-$) compared to control (CTRL) or ZAP70 deletion (ZAP70$^-$). Cells were stimulated with anti-CD3, anti-CD28 and IL-2 for 48 h, or IL-7 for 48 h (unstimulated control) and T cell activation was assessed. **e**, $CD8^+$ T cells were gated on Live/Dead-aqua$^-$, then CD44$^+$ and CD62L$^-$. **f**, Expression of CD25 was quantified after gating on Live/Dead-aqua$^-$CD8$^+$. **g**, Expression of PD-1 was quantified after gating on Live/Dead-aqua$^-$ CD8$^+$. **h**, Polar metabolites were extracted from supernatants and glucose was measured by LC–MS. Depletion of extracellular glucose across conditions is shown, normalized to cell number. In **e**–**h**, $n = 4$ biologically independent samples; one-way ANOVA corrected for multiple comparisons (Dunnett test). **i**, Experimental scheme. WT $CD8^+$ T cells were stimulated with anti-CD3, anti-CD28 and IL-2 for 24 h (**j**), or 48 h (**k**–**n**) in the presence or absence of Soy PI (100 μM). **j**, Total (left) and percentage (right) PI saturation. $n = 3$ biologically independent samples; one-way ANOVA corrected for multiple comparisons (Tukey test) comparing saturated PI. **k**,**l**, Expression of CD25 (**k**) and CD69 (**l**) in Live/Dead-IR$^-$, CD8-Brilliant Violet 421$^+$ cells. $n = 4$ unstimulated and $n = 5$ stimulated biologically independent samples, representative of three independent experiments; one-way ANOVA corrected for multiple comparisons (Sidak test). **m**, $CD8^+$ T cells were gated on Live/Dead-aqua$^-$, then CD44$^+$ and CD62L$^-$. **n**, Intracellular expression of IFN-γ was quantified by flow cytometry. Cells were gated on Live/Dead-IR$^-$, CD8-Brilliant Violet 421$^+$. In **m** and **n**, $n = 5$ biologically independent samples; one-way ANOVA corrected for multiple comparisons (Sidak test). Error bars show the s.e.m.

https://doi.org/10.1038/s41590-023-01419-y

after activation (Fig. 3a), but in contrast to T_{eff} cells, this was due to an increase in polyunsaturated PIP_2 (Fig. 3b). Over the same time, there was no change in PI abundance or acyl chain saturation, suggesting that immediately after TCR activation PIP_2 was generated by phosphorylating polyunsaturated PI present in unactivated T cells (Fig. 3c). We next deleted CDIPT (CDIPT⁻), and as an additional control we deleted ZAP70 (ZAP70⁻), a critical tyrosine kinase for T cell activation (Fig. 3d and Extended Data Fig. 3a). CTRL and CDIPT⁻ T cells comprised a similar percentage of cells with an effector phenotype ($CD44^+CD62L^-$) 48 h after stimulation, which was higher than unstimulated or ZAP70⁻ cells (Fig. 3e). CTRL and CDIPT⁻ cells also similarly expressed activation markers CD25 (Fig. 3f) and programmed cell death protein-1 (PD-1, Fig. 3g). CTRL and CDIPT⁻ cells comparably utilized extracellular glucose over 48 h (Fig. 3h), indicating that CDIPT⁻ T cells undergo appropriate metabolic remodeling during T cell activation. To determine whether increasing the saturated PI pool impacts early $CD8^+$ T cell activation, we stimulated $CD8^+$ T cells in the presence of Soy PI (Fig. 3i). Soy PI enlarged the intracellular PI pool substantially and shifted the PI composition toward saturated (Fig. 3j). This increased saturated PI content had no effect on the expression of the activation markers CD25

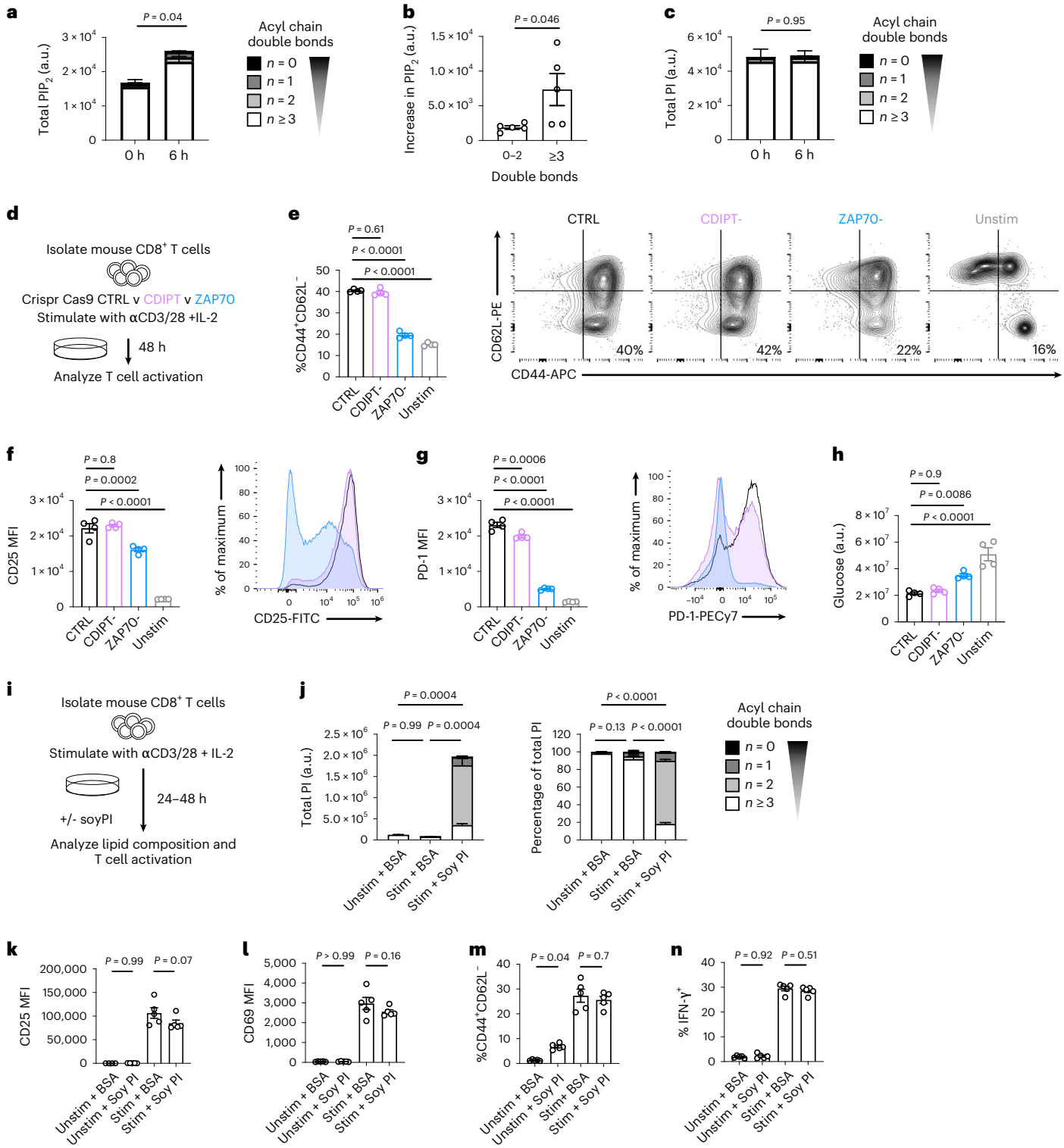

and CD69 48 h after T cell activation (Fig. 3k,l). Soy PI-supplemented T cells comprised similar percentages of $CD44^+CD62L^-$ cells (Fig. 3m) and had comparable IFN-γ production (Fig. 3n) 48 h after T cell activation. Therefore, while saturated PIP_n species are essential for fully differentiated T_{eff} cell fitness and function, hydrolysis of polyunsaturated PIP_n abundant in unactivated T cells is sufficient to mediate $CD8^+$ T cell activation early after TCR stimulation.

PIP_n acyl chain saturation potentiates late effector T cell signaling

While polyunsaturated PIP_2 exclusively supported early activation (Fig. 3a,b), saturated PIP_2 was essential for maintaining late T_{eff} cell function (Fig. 2c–g). Polyunsaturated PIP_2 remained abundant during CDIPT inhibition or deletion, but it was not sufficient to maintain T_{eff} cell function, highlighting the essential role of saturated PIP_n in T_{eff} cells. PIP_2 at the plasma membrane is continuously hydrolyzed by PLCγ1 to maintain sufficient levels of the second messengers DAG and IP_3 important for T_{eff} cell function[25] (Fig. 4a). To study whether depletion of the saturated PIP_2 pool would abrogate downstream signaling in T_{eff} cells, we analyzed PLCγ1-mediated signaling pathway activity upon CDIPT inhibition. Phosphorylated PLCγ1 expression or activity did not change in T_{eff} cells or in Jurkat cells (Fig. 4b and Extended Data Fig. 4a). In contrast, total DAG decreased (Fig. 4c). Downstream of DAG, p-Raf, p-MEK1/2 and p-ERK1/2 expression levels were decreased in CDIPTi-treated cells compared to CTRL cells (Fig. 4d,e). We were not able to measure IP_3 by LC–MS, but assessed downstream markers of IP_3 signaling. While intracellular basal Ca^{2+} levels were maintained, expression of F-actin was reduced in CDIPTi compared to CTRL cells (Fig. 4f,g). No difference in AKT phosphorylation suggests that PIP_3 signaling was unaffected by CDIPTi (Fig. 4h). These results support that saturated PIP_n is necessary to maintain PLCγ1-mediated signaling in T_{eff} cells.

We questioned how saturated PIP_n specifically maintains T_{eff} cell signaling, and speculated that distinct PIP_n pools might exist in different cellular compartments. We enriched distinct compartments from T_{eff} cells, and measured their lipid content. While PI localized to numerous organelles, PIP_2 was strongly enriched in lipid rafts (Fig. 4i,j). Of note, there was no compartment-specific difference in PIP_2 acyl chain saturation (Fig. 4i and Extended Data Fig. 4b), suggesting that preferential cellular localization was not an important driver of T_{eff} cell dependency on saturated PIP_n. To investigate how changes in PIP_n compare to changes in structural lipids in rafts, we measured the abundance of PI, phosphatidylserine (PS), sphingomyelin (SM) and gangliosides in T_{eff} cells and unstimulated $CD8^+$ T cells. We found that PI species and the ganglioside GM1 (but not GM2 or GM3) strongly increased, whereas PS species varied in expression and SM species decreased (Extended Data Fig. 4c). This suggested that increased PIP_2 in lipid rafts was not simply due to a general increase in all lipid components in rafts.

Lipid rafts are central to TCR signaling[26]. We questioned whether saturated PIP_n depletion affected raft formation. We observed decreased staining with cholera toxin subunit B, which binds to GM1 in lipid rafts[27], following CDIPTi in both T_{eff} cells and Jurkat cells (Extended Data Fig. 4d,e). Next, we used the fluorescent dye di-4-ANEPPDHQ[28] to examine membrane lipid order in T_{eff} cells treated with CDIPTi. CDIPT inhibition resulted in a higher emission at 630 nm, which correlated with a decreased fraction of cells with high lipid order and an increased fraction with low lipid order in both T_{eff} cells and Jurkat cells (Extended Data Fig. 4f,g). The generalized polarization (GP) value—a normalized intensity ratio of the two spectral emissions commonly used to quantify membrane lipid order—decreased in T_{eff} cells treated with CDIPTi (Extended Data Fig. 4h). We questioned whether changes in lipid raft formation and membrane lipid order were an immediate effect of saturated PIP_2 depletion or a secondary effect resulting from reduced PIP_2 signaling. At lower CDIPTi concentrations, cholera toxin B binding was less affected than MEK phosphorylation and IFN-γ production (Extended Data Fig. 4i). These data suggest that de novo synthesis of saturated PIP_2 is primarily required to maintain downstream PIP_2 signaling and thus $CD8^+$ T_{eff} cell function. Over longer times, synthesis of other lipid species and membrane lipid order are affected by CDIPTi as a consequence of diminished T_{eff} cell signaling.

PLCγ1 is activated by phosphorylation that occurs rapidly upon TCR ligation. We hypothesized that initial TCR stimulation would strongly activate PLCγ1, but that its activity would wane over time and in late T_{eff} cells, as signals from TCR stimulation dissipate, similar to what has been shown for other signaling pathways downstream of the TCR[19]. Supporting this idea, we observed that PLCγ1 phosphorylation decreased 72 h after activation, compared to 24 h after activation (Fig. 4k). In contrast, p-MEK1/2 and p-ERK1/2 expression was maintained (Fig. 4k), indicating that although PLCγ1 was less activated in late T_{eff} cells, downstream signaling was sustained. We hypothesized that this could be due to saturated PIP_n being a superior enzyme substrate compared to their polyunsaturated counterparts. We studied this in an in vitro phosphoinositide conversion assay, using supported lipid bilayers and purified components as previously described[29]. Briefly, membrane-coated beads comprising either PI(4)P 16:0/18:1 or PI(4)P 18:0/20:4 were distinctly labeled with NBD-DPPE or Atto647N-DOPE, respectively, and mixed. The PLC family recognizes its substrate, PI(4,5)P_2, through a conserved pleckstrin homology (PH) domain, which was fluorescently labeled and added to the membrane-coated beads. The main source of cellular PI(4,5)P_2 results from phosphorylation of PI(4)P into PI(4,5)P_2 by phosphatidylinositol 4-phosphate 5-kinases (PIP5K). To reconstitute this metabolic transition, recombinant PIP5K was added to the system at catalytic amounts, resulting in conversion of PI(4)P to PI(4,5)P_2 and subsequent recruitment of PLC-PH to the beads. PI conversion and subsequent PLC-PH recruitment to beads coated with bilayers containing PI(4)P 16:0/18:1 occurred almost twice

Fig. 4 | PIP_2 saturation potentiates effector T cell signaling. a, Schematic of PIP_2 signaling in T_{eff} cells. **b**–**g**, WT $CD8^+$ T cells were stimulated with anti-CD3, anti-CD28 and IL-2 for two d, treated with CTRL or CDIPTi (plus IL-2) for one d and then readouts of downstream signaling were measured. **b**, Expression of phosphorylated PLCγ1 (left) and activity of PLC enzyme (right). $n = 4$ biologically independent samples from two independent experiments; unpaired two-tailed *t*-test. **c**, Total DAG. $n = 4$ biologically independent samples representative of three independent experiments; unpaired two-tailed *t*-test. **d**, Protein expression of the Raf–MEK1/2–ERK1/2 signaling pathway. **e**, Relative intensity of p-ERK1/2-PE. $n = 3$ biologically independent samples; unpaired two-tailed *t*-test. **f**, Basal cytoplasmic calcium was calculated using the indo-AM dye bound/unbound ratio. $n = 3$ biologically independent samples; unpaired two-tailed *t*-test. **g**, Relative intensity of Phalloidin-AF647. $n = 4$ biologically independent samples; unpaired two-tailed *t*-test. **h**, Protein expression of the PI3K signaling pathway. **i**,**j**, WT $CD8^+$ T cells were stimulated with anti-CD3, anti-CD28 and IL-2 for two d, then a further two d in IL-2. Organelle compartments were enriched and PIP_n were extracted and analyzed by LC–QqQ–MS/MS or LC–QTOF–MS/MS. **i**, PI (upper) or PIP_2 (lower) saturation across organelles. $n = 4$ biologically independent samples. **j**, Heat map of the relative amount of saturated PIP_2 across organelles. $n = 4$ biologically independent samples; one-way ANOVA corrected for multiple comparisons (Dunnett test) comparing all groups with the lipid rafts. **k**, WT $CD8^+$ T cells were stimulated with anti-CD3, anti-CD28 and IL-2 for 24 h or 72 h (the final 24 h of which were only with IL-2). Expression of total and phosphorylated PLCγ1, MEK1/2 and ERK1/2 with tubulin as the loading control. $n = 4$ biological replicates pooled into one lane. **l**, Lower left, experimental schematic. Membrane-coated beads were generated by mixing liposomes (harboring 16:0–18:1 PI(4)P or 18:0–20:4 PI(4) together with 0.1% Atto647N-DOPE or NBD-DPPE) and silica beads. Purified PLC-PH fused to RFP was added, followed by PIP5K1C immediately before acquisition. Upper microscopy images. Lower right, recruitment of PLC measured by the normalized MFIs of the RFP signal to either of the membrane-coated bead populations, segmented using the NBD or Atto647N signal. $n = 40–50$ individual beads. Error bars show the s.e.m.

https://doi.org/10.1038/s41590-023-01419-y

as fast as to beads coated with PI(4)P 18:0/20:4 (Fig. 4l), indicating that PIP5K-mediated phosphorylation and/or PLC recruitment occurred more efficiently with saturated PIP_n compared to polyunsaturated PIP_n (Fig. 4l). The data from this assay show that saturated PIP_n are either superior enzyme substrates for PIP5K, or PLCγ1 recruitment to them is faster, as compared to polyunsaturated PIP_n. This 'preferential

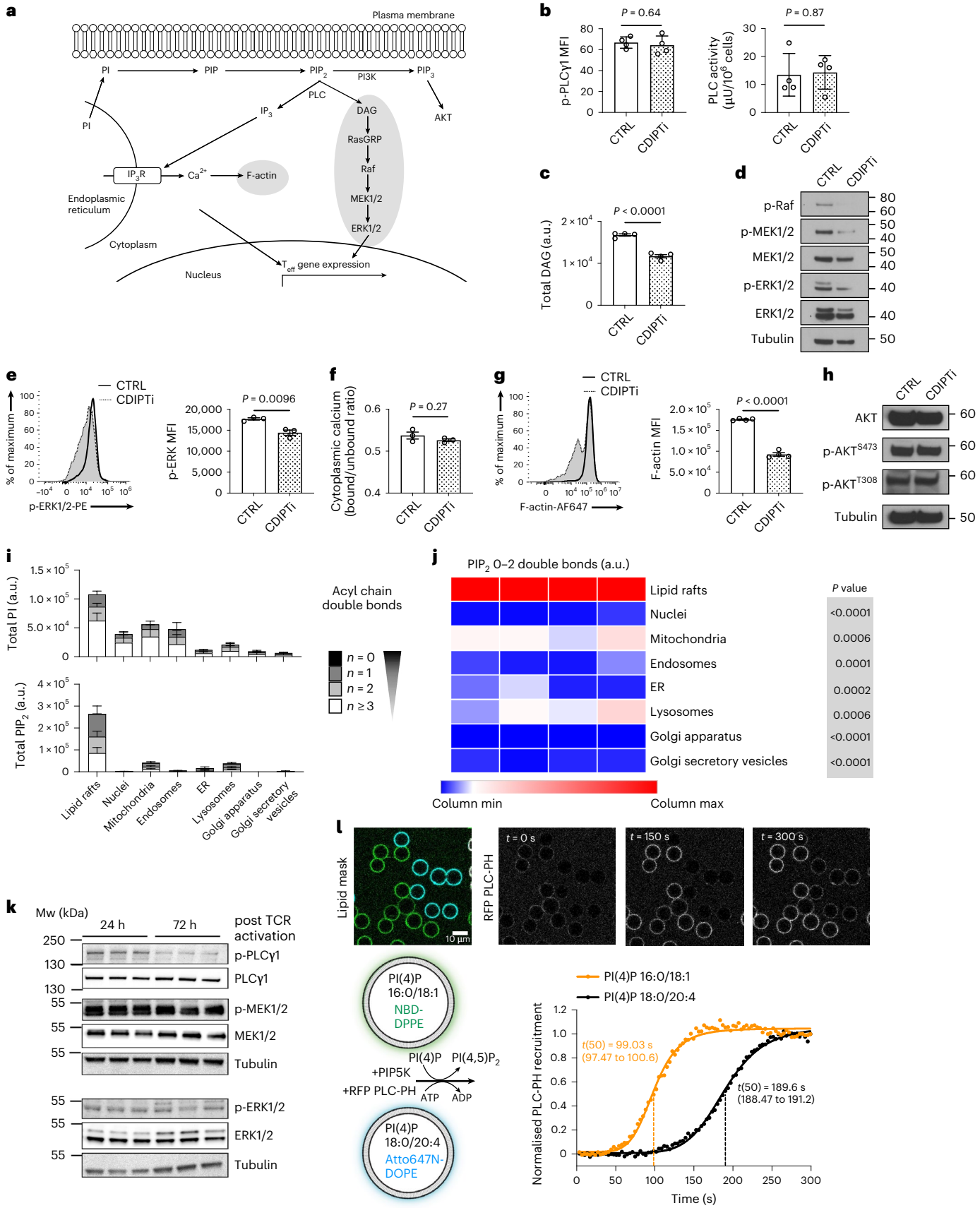

usage' of saturated PIP_n suggests why their presence is needed to maintain T cell signaling and function in late T_{eff} cells with waning PLCγ1 phosphorylation.

Effector T cell PIP_n synthesis is dependent on glycolytic metabolism

To understand which metabolic events drive synthesis of saturated PIP_n in T_{eff} cells, we measured PI every 24 h from 0–72 h after stimulation. Concentration of polyunsaturated PI species (predominantly PI 38:4) increased from 0 h to 48 h; however, after 48 h, those with 0–2 double bonds increased and shifted the PI composition toward saturated (Fig. 5a). De novo PI synthesis requires three substrates—two fatty acyl chains, a glycerol phosphate backbone and an inositol head group (Fig. 5b)—that may be directly acquired from the extracellular milieu or synthesized de novo from glucose. Following de novo synthesis, PI may be further remodeled, which involves cleavage of a saturated acyl chain to form LPI, then addition of a polyunsaturated fatty acid, which most commonly is arachidonic acid (Fig. 5b). We first assessed if differential enzyme expression in the de novo and remodeling pathways led to saturated PI accumulation. CDIPT levels did not change during the 72-h activation course (Fig. 5c), and two important enzymes in the remodeling pathway, lysocardiolipin acyltransferase (LYCAT, encoded by *Lclat1*)[30,31] and lysophosphatidylinositol acyltransferase (LPIAT, encoded by *Mboat7*)[32] showed elevated transcription after activation, suggesting that increased saturated PI was not due to a deficiency in the remodeling pathway machinery (Extended Data Fig. 5a). We also queried whether saturated PI accumulated due to a deficiency in linoleic acid (LA), an essential substrate for arachidonic acid synthesis and therefore polyunsaturated PI; however, LA treatment 48–72 h after stimulation did not reduce the proportion of PI with 0–2 double bonds (Fig. 5d). Stearoyl-CoA desaturase (SCD) synthesizes monounsaturated fatty acids (with one double bond). SCD inhibition decreased the proportion of saturated PI, which was rescued by oleic acid (OA; 18:1) addition (Fig. 5d). SCD inhibition also impaired T cell proliferation and cytokine production (Extended Data Fig. 5b). These findings indicate that saturated PI synthesis occurs between 48 and 72 h after T cell activation, depends on the de novo synthesis of fatty acids with one double bond, and is not caused by a deficiency in PI remodeling pathway enzymes or substrate.

Glucose is an important substrate for de novo fatty acid synthesis. Saturated PI species appeared late during $CD8^+$ T cell activation (Fig. 5a), a time that correlated with increased glucose uptake (Fig. 5e) and glycolytic metabolism, as determined by elevated lactate export (Fig. 5f). To test whether extracellular glucose was critical for de novo synthesis of saturated PI, we cultured mouse $CD8^+$ T cells in 10 mM or 1 mM glucose during the final 24 h of activation (Fig. 5g). PI composition shifted toward polyunsaturated in low glucose (Fig. 5h), indicating that glucose availability is important for de novo PI synthesis. With the same experimental setup (Fig. 5i), we inhibited hexokinase with 2-deoxy-glucose (2-DG) or glyceraldehyde 3-phosphate dehydrogenase (GAPDH) with koningic acid (KA), and observed a similar shift in PI toward polyunsaturated (Fig. 5j). Interestingly, GAPDH inhibition would still allow inositol and glycerol phosphate synthesis from glucose, but not de novo fatty acid synthesis, highlighting the importance of de novo fatty acid synthesis in saturated PI generation.

To show that glucose is a substrate for PI synthesis, we cultured cells in 10 mM or 1 mM uniformly labeled ^{13}C (U-^{13}C)-glucose for the last 24 h of culture (Fig. 5k). Using this long 24-h labeling time, we could determine the maximum fractional contribution of glucose carbon to PI: ~80% for PI 36:1 and ~70% for PI 36:2, which was reduced in 1 mM U-^{13}C-glucose, and was <1% in unlabeled glucose (Fig. 5l). U-^{13}C-glucose also contributed carbons to PI 38:4 (Fig. 5l), indicating that T_{eff} cells also actively maintain PI acyl chain remodeling (Fig. 5b,h). To compare the dynamics of PI and PIP_2 synthesis, we traced U-^{13}C-glucose into T_{eff} cells for 6 h (Fig. 5m,n). ^{13}C incorporation into PI 36:1 and PI 36:2 was ~5 times higher than into PI 38:4 (Fig. 5m). ^{13}C incorporation into PIP_2 36:1 and PIP_2 36:2 was ~8 times and ~11 times higher than into PIP_2 38:4, respectively (Fig. 5n). These data confirm that in T_{eff} cells, de novo saturated PI and PIP_2 synthesis occurs more rapidly than polyunsaturated PI and PIP_2. Increased PIP_n synthesis may be critical for maintaining downstream T_{eff} cell signaling during T_{eff} cell expansion, when high PIP_n amounts are required to support intensive proliferation. To test whether rapid proliferation is directly linked to a saturated PI pool, we activated $CD8^+$ T cells for 72 h at two different cell concentrations: 0.6×10^6 cells/ml, which allowed for sufficient cell–cell contact to support robust T_{eff} cell expansion, and at a fivefold lower concentration, where cell contact was inhibited (Fig. 5o). This approach allowed us to limit proliferation without potentially toxic pharmacological intervention that may also rewire cellular metabolism. Reduced proliferation aligned with a substantially decreased percentage of saturated PI (Fig. 5p), suggesting that rapid T_{eff} cell proliferation drives the de novo saturated PIP_n synthesis.

We next tested when glucose contributes to de novo PI synthesis. We measured incorporation of U-^{13}C-glucose into PI species every 24 h after $CD8^+$ T cell stimulation. During the first 24 h, we found no difference in the fractional contribution of U-^{13}C-glucose to PI production between unstimulated and stimulated $CD8^+$ T cells (Fig. 5q). However, at 48 and 72 h after activation, U-^{13}C-glucose became a major substrate for PI synthesis and contributed to ~80% of PI 36:1 (Fig. 5q), confirming that de novo PI synthesis occurs late during T cell activation, after T_{eff} cells have engaged glycolytic metabolism (Fig. 5e,f). These data also indicate that the turnover of PI species occurs at least every 24 h during the second and third day after $CD8^+$ T cell activation. T_{eff} cells are dependent on glycolytic metabolism to support their proliferation and function,

Fig. 5 | Effector T cell PIP_n synthesis depends on glycolytic metabolism. **a**, PI saturation (left) and percentage PI saturation (right) during WT $CD8^+$ T cell stimulation. $n = 3$ biologically independent samples representative of 3 independent experiments; one-way ANOVA corrected for multiple comparisons (Dunnett test) comparing saturated PI with the 0 h time point. **b**, Schematic of de novo PI synthesis. **c**, Protein expression of CDIPT, as in **a**. $n = 3$ biologically independent samples pooled into one sample. **d**, WT $CD8^+$ T cells were stimulated for 2 d, then for a further 24 h with BSA or BSA-conjugated LA (50 μM; left), or A939572 (SCDi; 100 nM), BSA-conjugated OA (100 μM), or a combination of both (right; plus IL-2), and PI saturation is shown. $n = 4$ or $n = 3$ biologically independent samples, respectively; unpaired two-tailed *t*-test or one-way ANOVA corrected for multiple comparisons (Tukey test) respectively on saturated PI. **e**,**f**, Glucose uptake and lactate export respectively, as in **a**. $n = 3$ biologically independent samples; one-way ANOVA corrected for multiple comparisons (Dunnett test) comparing each time point with the 0-h time point. **g**, Experimental schematic. **h**, Total PI saturation. $n = 3$ biologically independent samples; unpaired two-tailed *t*-test on saturated PI. **i**, Experimental schematic. **j**, Total PI saturation. $n = 3$ biologically independent samples; one-way ANOVA corrected for multiple comparisons (Dunnett test) comparing all groups with the vehicle control. **k**, Experimental schematic. **l**, Fractional ^{13}C incorporation into major PI species. $n = 3$ biologically independent samples; two-way ANOVA corrected for multiple comparisons (Sidak test). **m**,**n**, As in **k** with 6-h labeling. Fractional ^{13}C incorporation into major PI (**m**) or PIP_2 (**n**) species from U-^{13}C-glucose normalized to unlabeled glucose. $n = 3$ biologically independent samples; one-way ANOVA corrected for multiple comparisons (Tukey test). **o**,**p**, WT $CD8^+$ T cells were stained with CTV, activated as in **a**, and plated at 0.6×10^6 cells/ml or 0.12×10^6 cells/ml. **o**, Left, CTV dilution after 72 h of activation. Right, replication index. $n = 5$ biologically independent samples; unpaired two-tailed *t*-test. **p**, Total PI saturation. $n = 5$ biologically independent samples; unpaired two-tailed *t*-test comparing saturated PI. **q**, Fractional contribution of ^{13}C-glucose-derived carbon to PI major species as in **a**, with the addition of 100% U-^{13}C-glucose 24 h before lipid analysis at each time point. $n = 3$ biologically independent samples; two-way ANOVA corrected for multiple comparisons (Dunnett test) comparing respective PIs within each group with unstimulated cells. Error bars show the s.e.m.

https://doi.org/10.1038/s41590-023-01419-y

but they reduce glycolytic rates during IL-15-driven differentiation into memory T (T_M) cells[33]. We compared the PI 36:2 and PIP_2 pools of T_{eff} cells and T_M cells differentiated in vitro and found that T_M cells decreased saturated PI and PIP_2 and had a similar PIP_n composition to unstimulated T cells (Extended Data Fig. 5c,d). Upon stimulation, T_M cells engage glycolytic metabolism and effector function more rapidly than naive T cells[33]. Following stimulation, T_M cells rapidly increased PI 36:2 (Extended Data Fig. 5c). Furthermore, T_M incorporated U-^{13}C-glucose into PI within the first 24 h of secondary stimulation with anti-CD3/CD28 plus IL-2 (Extended Data Fig. 5e). Collectively, these data show that de novo saturated PI synthesis depends on extracellular glucose and enhanced glycolytic metabolism, linking nutrient availability to

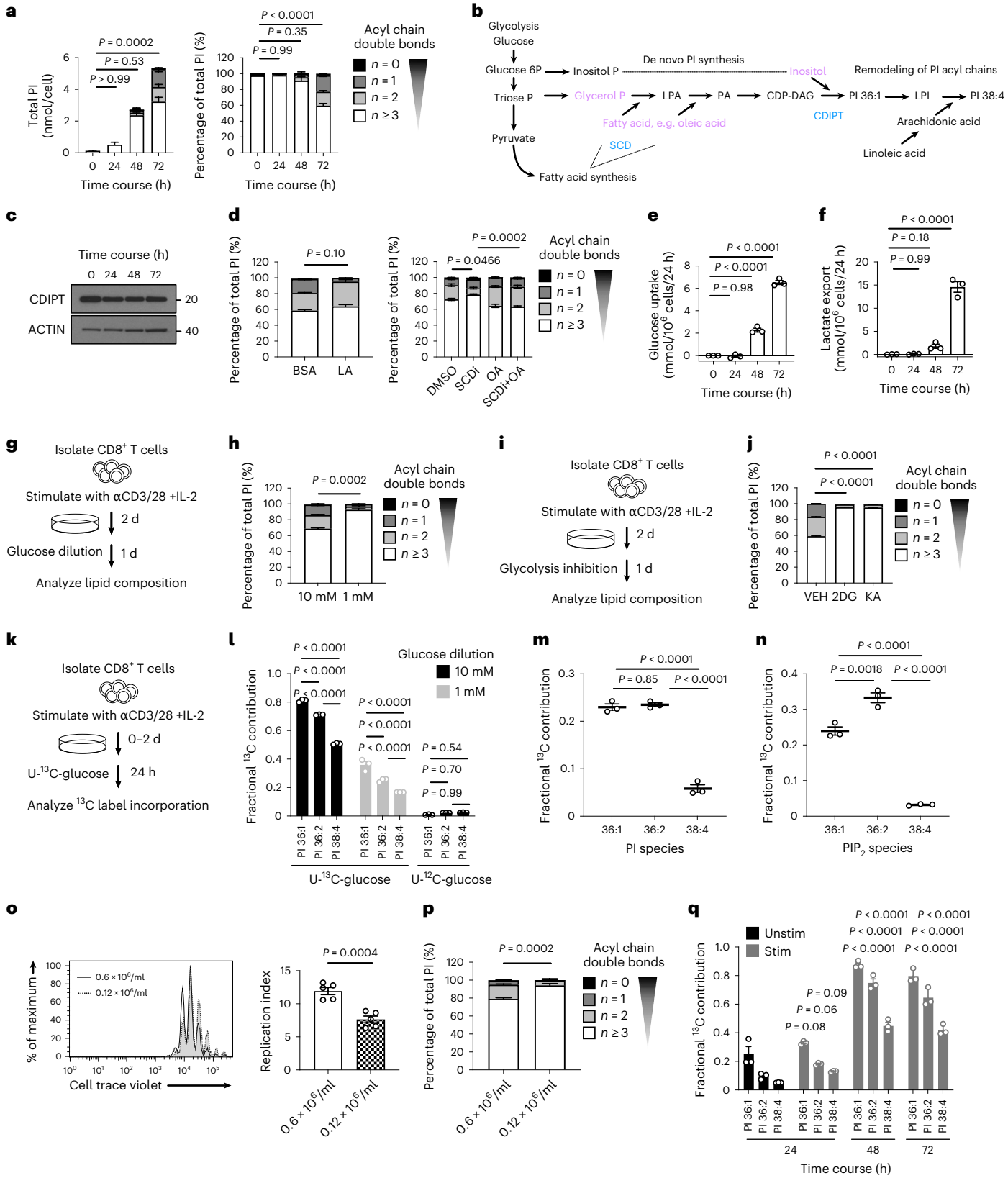

https://doi.org/10.1038/s41590-023-01419-y

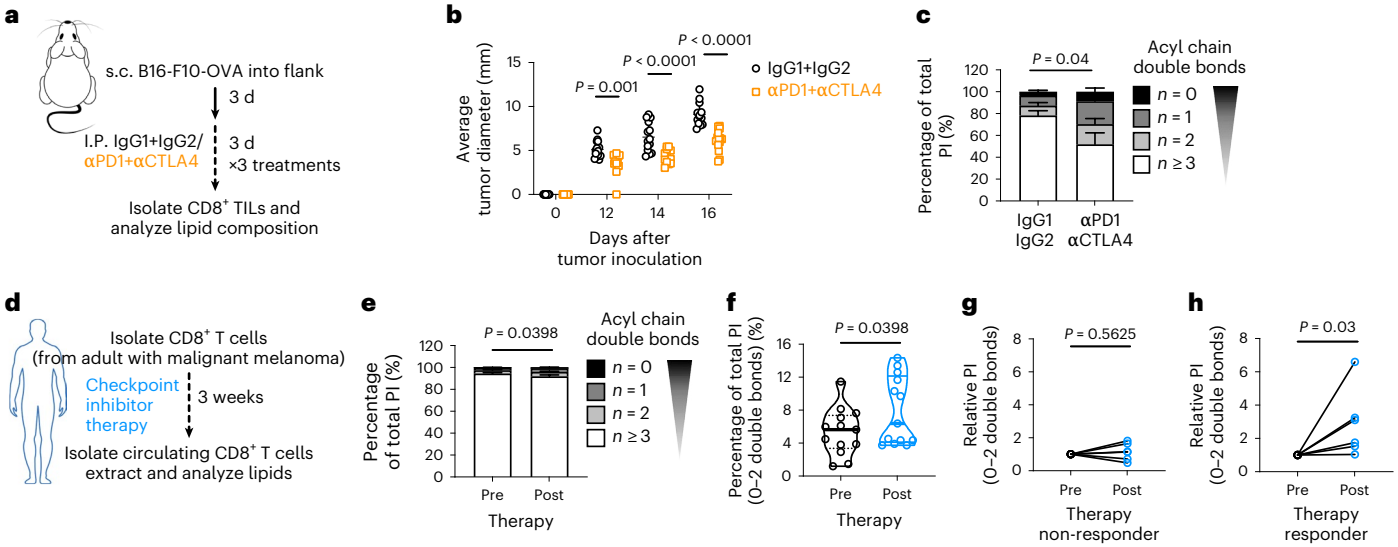

Fig. 6 | Immunotherapy-boosted tumor-infiltrating lymphocytes synthesize saturated PI. a–c, Sex-matched C57BL/6 mice were injected in the right flank with 1×10^6 B16-F10-OVA cells. After three d, mice were given intraperitoneal injections of anti-PD-1 and anti-CTLA4 (aPD1 + aCTLA4) or matching isotype controls (IgG1 + IgG2) every three d for three rounds in total. Tumor growth was measured up to day 16 after tumor injection and CD8$^+$ T cells were isolated on day 12 after tumor injection to measure T cell function and lipid composition. **b**, Average tumor diameter at indicated time points. $n = 14$ biologically independent animals; two-way ANOVA corrected for multiple comparisons (Sidak test) comparing the two groups at each time point across the dataset. **c**, Lipids were analyzed from TILs on day 12 after tumor injection. Saturation of acyl chains is expressed as a percentage of total PI. Statistical analysis was carried out on the summed percentage of saturated PI on $n = 7$ IgG1 + IgG2 and $n = 8$ aPD1 + aCTLA4 biologically independent samples using an unpaired two-tailed *t*-test. **d–h**, CD8$^+$ T cells were isolated from the blood of adult participants with histologically confirmed stage III or IV malignant melanoma ($n = 13$) on the day of immune checkpoint inhibitor treatment initiation (before therapy, "pre") and then when the participant presented for the second administration of treatment (after therapy, "post"). Long-term disease response (non-responder versus responder) to checkpoint inhibitor treatment was assessed (median follow-up time of 318 d). Lipids were extracted and analyzed by LC–QqQ–MS/MS. **e**,**f**, Lipids were analyzed before and after therapy. Saturation of acyl chains is expressed as a percentage of total PI. Statistical analysis was carried out on the summed percentage of saturated PI using a two-tailed Wilcoxon matched-pairs signed-rank test ($n = 13$). **g**,**h**, Lipids were analyzed and grouped by response to therapy. Relative intensity of saturated PI species normalized to pre-therapy level is shown. Statistical analysis was carried out using a two-tailed Wilcoxon matched-pairs signed-rank test ($n = 6$ responders and $n = 6$ non-responders). Error bars show the s.e.m. s.c., subcutaneous.

T_{eff} cell signaling. Notably, glucose carbon incorporation into saturated PI and PIP_2 occurs faster than into polyunsaturated counterparts, indicating that reaction speed might be critical to maintain the PIP_n pool and support signaling in rapidly expanding T_{eff} cells.

Immunotherapy-boosted tumor-infiltrating lymphocytes synthesize saturated PI

Expression of the inhibitory receptors PD-1 and cytotoxic T lymphocyte-associated protein 4 (CTLA4) decreases CD8$^+$ T cell glucose uptake and glycolysis[34]. We previously demonstrated that PD-1 blockade reverses glucose restriction in CD8$^+$ TILs, which restores IFN-γ expression and antitumor function[35]. Here, we show that glucose is an essential substrate for de novo saturated PIP_n synthesis (Fig. 5g–q). We hypothesized that TILs with restored glycolytic metabolism and boosted function after checkpoint inhibitor therapy would synthesize saturated PI. We compared TILs from mice bearing B16-F10-OVA melanoma tumors treated with three rounds of isotype controls (IgG1 + IgG2) or combined checkpoint inhibitor therapy anti-PD-1 plus anti-CTLA4 (αPD-1 + αCTLA4; Fig. 6a). αPD-1 + αCTLA4-treated mice had smaller tumors compared to IgG1 + IgG2-treated mice (Fig. 6b), and their CD8$^+$ TILs expressed more IFN-γ and granzyme B (Extended Data Fig. 6a–c). CD8$^+$ TILs isolated from αPD-1 + αCTLA4-treated mice 12 d after tumor injection had increased saturated PI composition compared to IgG1 + IgG2-treated mice (Fig. 6c). The total amount of PI was equal between groups (Extended Data Fig. 6d). Next, we questioned whether tumors with different sensitivity to checkpoint blockade have specific changes in the PI saturation of their TILs. We treated mice bearing B16-F10-OVA melanoma tumors with three rounds of anti-PD-1 antibody alone and found that tumor size was not reduced (Extended Data Fig. 6e) and the TILs did not show a shift in PI saturation (Extended Data Fig. 6f), indicating that only CD8$^+$ TILs with improved antitumor function following checkpoint inhibitor therapy are marked by increased saturated PI.

Immune checkpoint inhibitors are a frontline treatment for patients with advanced melanoma[36]. We questioned whether an increase in saturated PI could be detected in peripheral blood CD8$^+$ T cells of participants undergoing immunotherapy. We isolated circulating CD8$^+$ T cells from adults with stage III or stage IV melanoma before and after the first round of checkpoint inhibitor therapy (Fig. 6d). We measured CD8$^+$ T cell lipids and observed a shift in PI composition toward saturation after therapy (Fig. 6e,f). We then analyzed the clinical and radiological assessments of disease courses with a median follow-up time of 318 d (range 184–484 d). Per the radiologist's assessment, we divided participants into non-responder (stable or progressive disease) and responder (partial or complete remission) groups. In the non-responder group, we observed no relative increase in saturated PI species (Fig. 6g), while in the responder group we observed a statistically significant increase (Fig. 6h). Therefore, early changes in PI composition may correlate with successful long-term response to checkpoint inhibitor therapy in patients with advanced melanoma.

Discussion

We analyzed the lipidome and found that PI with a distinct acyl chain composition marked by a reduced number of double bonds accumulated in T_{eff} cells. We discovered that two separate PIP_n pools—one saturated with 0–2 double bonds, and one polyunsaturated with ≥3 double

https://doi.org/10.1038/s41590-023-01419-y

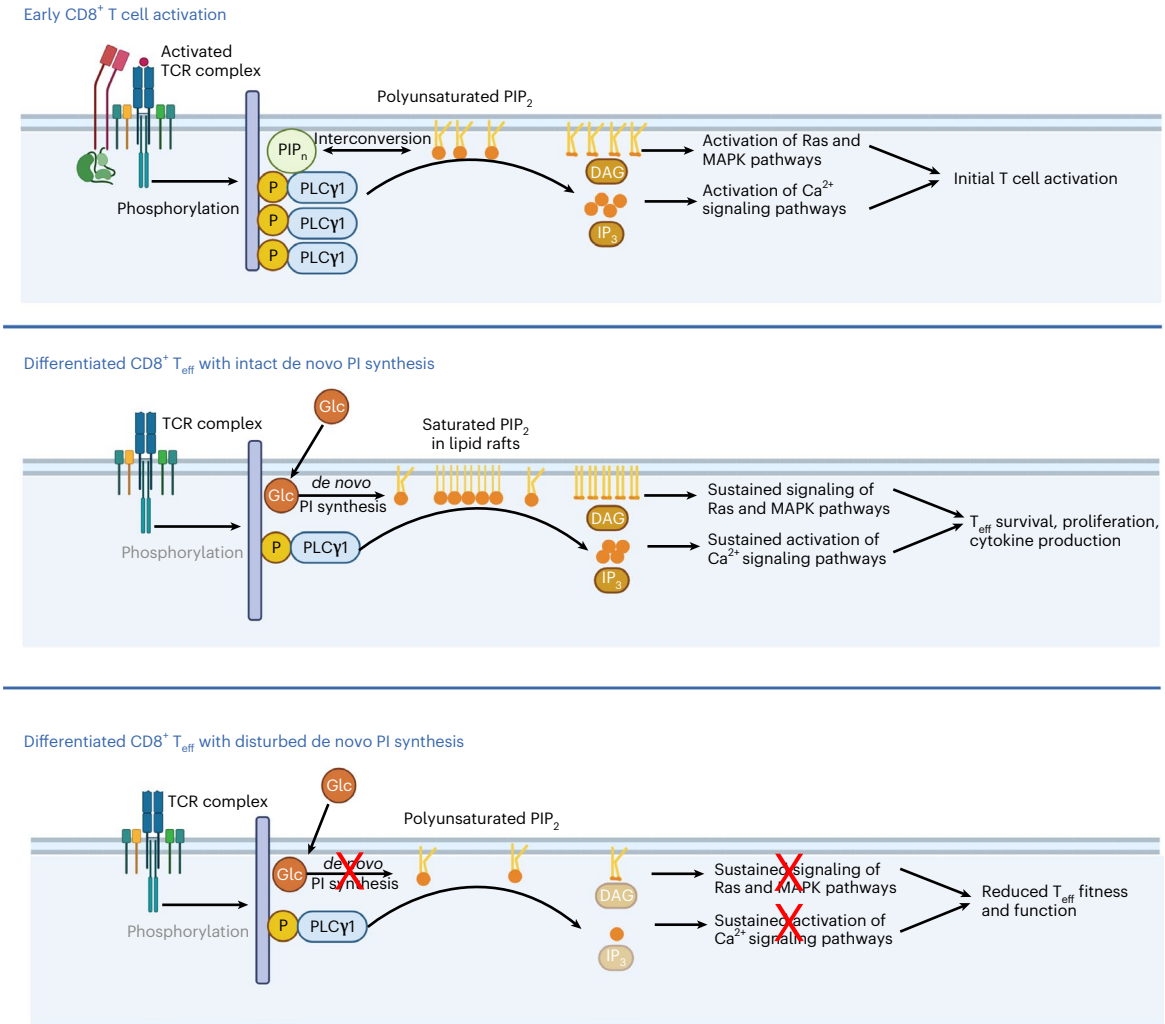

Fig. 7 | PIP_2 saturation defines early activation versus late effector T cell signaling. Early $CD8^+$ T cell activation is marked by a robust phosphorylation of PLCγ1, which cleaves polyunsaturated PIP_2 to generate the second messengers DAG and IP_3. In fully differentiated $CD8^+$ T_{eff} cells, PLCγ1 phosphorylation decreases as TCR signals dissipate; and a lipid raft-accumulated saturated PIP_2 pool, synthesized de novo from glucose, becomes essential for sustained signaling and T_{eff} cell survival, proliferation and cytokine production. When de novo PI synthesis is inhibited, the saturated PIP_2 pool is specifically depleted, and this results in disturbed downstream signaling and reduced T_{eff} cell fitness and function. Glc, glucose; MAPK, mitogen-activated protein kinase; T_{eff}, $CD8^+$ T_{eff} cell. Created with BioRender.com.

bonds—drive important signaling events at specific stages of T_{eff} cell differentiation. Sustained T_{eff} cell signaling is driven by saturated PIP_n, while polyunsaturated PIP_n are exclusively utilized early during T cell activation. Saturated PIP_n synthesis only occurred late during T_{eff} cell differentiation, which might be necessary to sustain DAG production and downstream signaling as TCR-driven PLCγ1 activation waned. T_{eff} cell PIP_n signaling was maintained (1) by the rapid and continuous de novo saturated PI synthesis from glucose, facilitated by T_{eff} cell glycolytic metabolism; and (2) by the preference of PIP5K and/or PLC for more saturated PIP_n, or their association with more saturated PIP_n, even in the presence of abundant polyunsaturated PIP_n. The dependence on extracellular glucose for PIP_n synthesis directly ties the nutrient environment with T_{eff} cell signaling. Finally, T cells with improved antitumor function following checkpoint inhibitor therapy synthesized more saturated PIP_n in mouse and human melanoma.

Rapid interconversion and salvage of polyunsaturated PIP_n following TCR ligation and co-stimulation is critical for initiating signaling and T cell activation[25,37]. However, how PIP_n signaling is maintained during differentiation into T_{eff} cells with increased biosynthetic demands, along with the diminution of TCR signaling[38,39] is unknown. Mammalian PIP_n is unique among other lipids in its characteristic fatty acid profile enriched in PIP_n 38:4, with stearic acid (18:0) at the sn-1 position and arachidonic acid (20:4) at the sn-2 position[8]. We found that in contrast to the first hours after activation, when polyunsaturated PIP_2 is prevalent, $CD8^+$ T_{eff} cells augmented saturated PIP_n synthesis 24–48 h after stimulation, which increased the total PI and PIP_2 pool, while the polyunsaturated PIP_2 pool remained constant. Increased PIP_n saturation has been observed in transformed cell lines[40,41], which may indicate that saturated PIP_n synthesis drives PIP_n signaling in cell types with increased biosynthetic demands.

T_{eff} cell function is dependent on metabolic reprogramming involving increased glucose metabolism[42,43]. T_{eff} cell glycolytic metabolism was previously linked to downstream PIP_2 signaling, as increased phosphoenolpyruvate synthesis inhibits SERCA-dependent calcium reuptake, thus maintaining increased cytoplasmic calcium and NFAT1 signaling[44]. Here we report that glycolytic metabolism directly regulates PIP_2 signaling, as glucose is the predominant substrate for de novo saturated PIP_n synthesis, meaning that PIP_2 signaling is dependent on glucose availability and enhanced T_{eff} cell glycolytic metabolism. We measured the de novo synthesis of PI with different acyl chain

compositions using U-^{13}C-glucose and found that saturated PI synthesis occurs more rapidly, in keeping with recent findings[45], as does saturated PI phosphorylation to PIP_2 by PIP5K. Notably, PIP5K exhibits acyl chain preference. The Michaelis constant, which denotes the substrate concentration at which an enzyme reaches half its maximum rate, is lower for PIP 36:1 compared to PIP 38:4[46], supporting our findings that T_{eff} cells synthesize saturated PIP_2 more rapidly than polyunsaturated PIP_2. We measured the conversion of PI(4)P 16:0/18:1 versus 18:0/20:4 to PI(4,5)P_2, and concomitant recruitment of PLC and demonstrated that this process occurred almost twice as fast for PI(4)P 16:0/18:1 as for PI(4)P 38:4. Thus, increased de novo synthesis of saturated PIP_n from glucose directly links PIP_n signaling to T_{eff} cell glycolytic metabolism, and is critical to maintain a higher rate of PIP_n turnover in T_{eff} cells.

CDIPT exchanges inositol for CMP on CDP-DAG in the final step of de novo PI synthesis[47]. CDIPT is not known to have acyl chain selectivity[48], suggesting that the regulation of PIP_n acyl chain composition occurs during de novo fatty acid synthesis. Supplementing T_{eff} cells with LA did not increase polyunsaturated PI synthesis, indicating that saturated PI synthesis does not occur due to a lack of substrate for arachidonic acid synthesis. Furthermore, our data suggest that expression of enzymes in the PI remodeling pathway are intact[30–32]. CDIPT inhibition or deletion specifically inhibited de novo saturated PI and PIP_2 synthesis. PLCγ1 expression and activity were maintained after CDIPT inhibition, but downstream of PIP_2 there was decreased DAG, p-Raf, p-MEK1/2 and p-ERK1/2. Interestingly, while the polyunsaturated PI pool was maintained during CDIPT inhibition, likely due to remodeling of LPI to PI 38:4, polyunsaturated PI was not phosphorylated to PIP_2, and the total PIP_2 content was halved. Thus, de novo PI synthesis in T_{eff} cells predominantly supports the saturated pool, while the polyunsaturated pool is maintained even when CDIPT is inhibited or deleted.

We also found that PIP_2 exhibited a strong preference for lipid rafts, potentially because in this compartment phospholipids with more saturated acyl chains are able to pack closer with the saturated acyl chains of sphingolipids[49], and hence can be efficiently hydrolyzed by PLCγ1. PLCγ1 depletes PIP_2 and produces DAG more rapidly in lipid domains with high order versus low order[50], and PLCγ1 activation is regulated by lipid rafts[51]. CDIPT inhibition reduced lipid order and lipid raft formation in T_{eff} cells. A decrease in lipid raft formation might be caused directly by disturbed cytoskeleton remodeling in the absence of PIP_2. In fact, PIP5Kβ, one of the main PIP_2-generating enzymes, regulates actin reorganization required for lipid raft recruitment at the immunological synapse of $CD4^+$ T cells[52]. Notably, PLCγ1 phosphorylation was lower in T_{eff} cells 72 h after activation compared to 24 h, and we believe that the efficient synthesis and hydrolysis of saturated PIP_2 is essential to sustain signaling in late T_{eff} cells. The functional consequence of a diminished saturated PIP_2 pool in T_{eff} cells was reduced viability, proliferation and effector function. Therefore, glycolysis-driven de novo saturated PIP_n synthesis is central to T_{eff} cell function.

$CD8^+$ T_{eff} cells can kill malignant cells; however, tumor-imposed metabolic restrictions that affect T_{eff} cell glycolytic metabolism can hamper $CD8^+$ T cell antitumor function and permit tumor progression[35,44]. We found that saturated PI synthesis was increased in $CD8^+$ TILs, and CDIPT was required for $CD8^+$ TIL antitumor fitness and function. A common feature of TILs is increased inhibitory checkpoint receptor (for example, PD-1 and CTLA4) expression that impairs TCR signaling and glycolytic metabolism[53]. Checkpoint inhibitor therapy has shown promise in many advanced cancers[36,54]. We observed increased PI saturation after immunotherapy in both mouse TILs and circulating $CD8^+$ T cells isolated from participants with melanoma who responded to checkpoint inhibitor treatment, indicating that saturated PI may be a characteristic of functional T_{eff} cells in a clinical setting.

In summary, diverse pools of PIP_n with differing acyl chain saturation are critical regulators of distinct $CD8^+$ T cell differentiation programs. Polyunsaturated PIP_2 (≥3 double bonds) sufficiently supports T cell signaling early after TCR stimulation when cells have limited proliferation rates and recent TCR activation triggers abundant PLCγ1 phosphorylation. As $CD8^+$ T cells commit to their full T_{eff} cell function marked by intense proliferation and an increased demand for second messengers in the light of waning PLCγ1 activity, rapid synthesis and conversion of saturated PIP_n from glucose becomes essential for sustained T_{eff} cell signaling. As such, inhibition of saturated PIP_n synthesis impairs T_{eff} cell fitness and function in infection and cancer (Fig. 7). Thus, fatty acid chain saturation in PIP_n is a new mechanism that governs T cell signaling at different stages of $CD8^+$ T cell differentiation. Given the central role of T_{eff} cells in antitumor immunity and in autoimmune diseases, our findings may provide an avenue for modulating PIP_n saturation as a means to balance T_{eff} cell activity.

Online content

Any methods, additional references, Nature Portfolio reporting summaries, source data, extended data, supplementary information, acknowledgements, peer review information; details of author contributions and competing interests; and statements of data and code availability are available at https://doi.org/10.1038/s41590-023-01419-y.

References

1. Waickman, A. T. & Powell, J. D. mTOR, metabolism, and the regulation of T cell differentiation and function. *Immunol. Rev.* **249**, 43–58 (2012).
2. MacIver, N. J., Michalek, R. D. & Rathmell, J. C. Metabolic regulation of T lymphocytes. *Annu Rev. Immunol.* **31**, 259–283 (2013).
3. Shyer, J. A., Flavell, R. A. & Bailis, W. Metabolic signaling in T cells. *Cell Res* **30**, 649–659 (2020).
4. Carr, E. L. et al. Glutamine uptake and metabolism are coordinately regulated by ERK/MAPK during T lymphocyte activation. *J. Immunol.* **185**, 1037–1044 (2010).
5. Wang, R. et al. The transcription factor Myc controls metabolic reprogramming upon T lymphocyte activation. *Immunity* **35**, 871–882 (2011).
6. Maciver, N. J. et al. Glucose metabolism in lymphocytes is a regulated process with significant effects on immune cell function and survival. *J. Leukoc. Biol.* **84**, 949–957 (2008).
7. Cham, C. M. & Gajewski, T. F. Glucose availability regulates IFN-γ production and p70S6 kinase activation in $CD8^+$ effector T cells. *J. Immunol.* **174**, 4670–4677 (2005).
8. Barneda, D., Cosulich, S., Stephens, L. & Hawkins, P. How is the acyl chain composition of phosphoinositides created and does it matter? *Biochem. Soc. Trans.* **47**, 1291–1305 (2019).
9. Sasaki, T. et al. Mammalian phosphoinositide kinases and phosphatases. *Prog. Lipid Res.* **48**, 307–343 (2009).
10. Czech, M. P. PIP2 and PIP3: complex roles at the cell surface. *Cell* **100**, 603–606 (2000).
11. Huang, Y. H. & Sauer, K. Lipid signaling in T cell development and function. *Cold Spring Harb. Perspect. Biol.* **2**, a002428 (2010).
12. Berridge, M. J. Inositol trisphosphate and calcium signalling mechanisms. *Biochim. Biophys. Acta* **1793**, 933–940 (2009).
13. D'Souza, W. N., Chang, C. F., Fischer, A. M., Li, M. & Hedrick, S. M. The Erk2 MAPK regulates CD8 T cell proliferation and survival. *J. Immunol.* **181**, 7617–7629 (2008).
14. Joseph, N., Reicher, B. & Barda-Saad, M. The calcium feedback loop and T cell activation: how cytoskeleton networks control intracellular calcium flux. *Biochim. Biophys. Acta* **1838**, 557–568 (2014).
15. Sun, Y., Dandekar, R. D., Mao, Y. S., Yin, H. L. & Wulfing, C. Phosphatidylinositol (4,5) bisphosphate controls T cell activation by regulating T cell rigidity and organization. *PLoS One* **6**, e27227 (2011).

16. Vickers, J. D. & Mustard, J. F. The phosphoinositides exist in multiple metabolic pools in rabbit platelets. *Biochem. J.* **238**, 411–417 (1986).
17. Chakrabarti, P. et al. A dPIP5K dependent pool of phosphatidylinositol 4,5 bisphosphate (PIP2) is required for G-protein-coupled signal transduction in *Drosophila* photoreceptors. *PLoS Genet.* **11**, e1004948 (2015).
18. Fujita, A., Cheng, J., Tauchi-Sato, K., Takenawa, T. & Fujimoto, T. A distinct pool of phosphatidylinositol 4,5-bisphosphate in caveolae revealed by a nanoscale labeling technique. *Proc. Natl Acad. Sci. USA* **106**, 9256–9261 (2009).
19. Costello, P. S., Gallagher, M. & Cantrell, D. A. Sustained and dynamic inositol lipid metabolism inside and outside the immunological synapse. *Nat. Immunol.* **3**, 1082–1089 (2002).
20. Latour, S. & Fischer, A. Signaling pathways involved in the T cell-mediated immunity against Epstein–Barr virus: lessons from genetic diseases. *Immunol. Rev.* **291**, 174–189 (2019).
21. Imoto, M., Taniguchi, Y. & Umezawa, K. Inhibition of CDP-DG: inositol transferase by inostamycin. *J. Biochem.* **112**, 299–302 (1992).
22. Bengsch, B. et al. Analysis of CD127 and KLRG1 expression on hepatitis C virus-specific $CD8^+$ T cells reveals the existence of different memory T cell subsets in the peripheral blood and liver. *J. Virol.* **81**, 945–953 (2007).
23. Ward, S. G. & Cantrell, D. A. Phosphoinositide 3-kinases in T lymphocyte activation. *Curr. Opin. Immunol.* **13**, 332–338 (2001).
24. Hawse, W. F. & Cattley, R. T. T cells transduce T cell receptor signal strength by generating different phosphatidylinositols. *J. Biol. Chem.* **294**, 4793–4805 (2019).
25. Hwang, J. R., Byeon, Y., Kim, D. & Park, S. G. Recent insights of T cell receptor-mediated signaling pathways for T cell activation and development. *Exp. Mol. Med.* **52**, 750–761 (2020).
26. Janes, P. W., Ley, S. C., Magee, A. I. & Kabouridis, P. S. The role of lipid rafts in T cell antigen receptor (TCR) signalling. *Semin. Immunol.* **12**, 23–34 (2000).
27. Holmgren, J., Lonnroth, I. & Svennerholm, L. Tissue receptor for cholera exotoxin: postulated structure from studies with GM1 ganglioside and related glycolipids. *Infect. Immun.* **8**, 208–214 (1973).
28. Waddington, K. E., Pineda-Torra, I. & Jury, E. C. Analyzing T cell plasma membrane lipids by flow cytometry. *Methods Mol. Biol.* **1951**, 209–216 (2019).
29. Maib, H. & Murray, D. H. A mechanism for exocyst-mediated tethering via Arf6 and PIP5K1C-driven phosphoinositide conversion. *Curr. Biol.* **32**, 2821–2833 (2022).
30. Zhao, Y., Chen, Y. Q., Li, S., Konrad, R. J. & Cao, G. The microsomal cardiolipin remodeling enzyme acyl-CoA lysocardiolipin acyltransferase is an acyltransferase of multiple anionic lysophospholipids. *J. Lipid Res.* **50**, 945–956 (2009).
31. Bone, L. N. et al. The acyltransferase LYCAT controls specific phosphoinositides and related membrane traffic. *Mol. Biol. Cell* **28**, 161–172 (2017).
32. Lee, H. C. et al. *Caenorhabditis elegans* mboa-7, a member of the MBOAT family, is required for selective incorporation of polyunsaturated fatty acids into phosphatidylinositol. *Mol. Biol. Cell* **19**, 1174–1184 (2008).
33. van der Windt, G. J. et al. CD8 memory T cells have a bioenergetic advantage that underlies their rapid recall ability. *Proc. Natl Acad. Sci. USA* **110**, 14336–14341 (2013).
34. Bengsch, B. et al. Bioenergetic insufficiencies due to metabolic alterations regulated by the inhibitory receptor PD-1 are an early driver of $CD8^+$ T cell exhaustion. *Immunity* **45**, 358–373 (2016).
35. Chang, C. H. et al. Metabolic competition in the tumor microenvironment is a driver of cancer progression. *Cell* **162**, 1229–1241 (2015).
36. Wolchok, J. D. et al. Nivolumab plus ipilimumab in advanced melanoma. *N. Engl. J. Med.* **369**, 122–133 (2013).
37. Hawse, W. F., Boggess, W. C. & Morel, P. A. TCR signal strength regulates Akt substrate specificity to induce alternate murine T_h and T regulatory cell differentiation programs. *J. Immunol.* **199**, 589–597 (2017).
38. Lee, K. H. et al. T cell receptor signaling precedes immunological synapse formation. *Science* **295**, 1539–1542 (2002).
39. Lee, K. H. et al. The immunological synapse balances T cell receptor signaling and degradation. *Science* **302**, 1218–1222 (2003).
40. Traynor-Kaplan, A. et al. Fatty-acyl chain profiles of cellular phosphoinositides. *Biochim. Biophys. Acta Mol. Cell Biol. Lipids* **1862**, 513–522 (2017).
41. Naguib, A. et al. p53 mutations change phosphatidylinositol acyl chain composition. *Cell Rep.* **10**, 8–19 (2015).
42. van der Windt, G. J. & Pearce, E. L. Metabolic switching and fuel choice during T cell differentiation and memory development. *Immunol. Rev.* **249**, 27–42 (2012).
43. Frauwirth, K. A. et al. The CD28 signaling pathway regulates glucose metabolism. *Immunity* **16**, 769–777 (2002).
44. Ho, P. C. et al. Phosphoenolpyruvate is a metabolic checkpoint of anti-tumor T cell responses. *Cell* **162**, 1217–1228 (2015).
45. Barneda, D. et al. Acyl chain selection couples the consumption and synthesis of phosphoinositides. *EMBO J.* **41**, e110038 (2022).
46. Shulga, Y. V., Anderson, R. A., Topham, M. K. & Epand, R. M. Phosphatidylinositol-4-phosphate 5-kinase isoforms exhibit acyl chain selectivity for both substrate and lipid activator. *J. Biol. Chem.* **287**, 35953–35963 (2012).
47. Blunsom, N. J. & Cockcroft, S. Phosphatidylinositol synthesis at the endoplasmic reticulum. *Biochim. Biophys. Acta Mol. Cel. Biol. Lipids* **1865**, 158471 (2020).
48. D'Souza, K. & Epand, R. M. The phosphatidylinositol synthase-catalyzed formation of phosphatidylinositol does not exhibit acyl chain specificity. *Biochemistry* **54**, 1151–1153 (2015).
49. Pike, L. J. Lipid rafts: bringing order to chaos. *J. Lipid Res.* **44**, 655–667 (2003).
50. Myeong, J., Park, C. G., Suh, B. C. & Hille, B. Compartmentalization of phosphatidylinositol 4,5-bisphosphate metabolism into plasma membrane liquid-ordered/raft domains. *Proc. Natl Acad. Sci. USA* **118**, e2025343118 (2021).
51. Veri, M. C. et al. Membrane raft-dependent regulation of phospholipase Cγ-1 activation in T lymphocytes. *Mol. Cell. Biol.* **21**, 6939–6950 (2001).
52. Kallikourdis, M. et al. Phosphatidylinositol 4-phosphate 5-kinase beta controls recruitment of lipid rafts into the immunological synapse. *J. Immunol.* **196**, 1955–1963 (2016).
53. Parry, R. V. et al. CTLA-4 and PD-1 receptors inhibit T cell activation by distinct mechanisms. *Mol. Cell. Biol.* **25**, 9543–9553 (2005).
54. Callahan, M. K., Postow, M. A. & Wolchok, J. D. Targeting T cell co-receptors for cancer therapy. *Immunity* **44**, 1069–1078 (2016).

[1]Max Planck Institute of Immunobiology and Epigenetics, Freiburg, Germany. [2]Bloomberg–Kimmel Institute for Cancer Immunotherapy and Department of Oncology, Johns Hopkins University School of Medicine, Baltimore, MD, USA. [3]Division of Cell & Developmental Biology, School of Life Sciences, University of Dundee, Dundee, UK. [4]Center for Chronic Immunodeficiency, Medical Center – University of Freiburg, Faculty of Medicine, University of Freiburg, Freiburg, Germany. [5]Clinic for Internal Medicine II, Gastroenterology, Hepatology, Endocrinology, and Infectious Diseases, Medical Center – University of Freiburg, Faculty of Medicine, University of Freiburg, Freiburg, Germany. [6]Faculty of Biology, University of Freiburg, Freiburg, Germany. [7]Department of Dermatology, Medical Center – University of Freiburg, Faculty of Medicine, University of Freiburg, Freiburg, Germany. [8]Signaling Research Centers BIOSS and CIBSS, University of Freiburg, Freiburg, Germany. [9]Department of Medicine I, Medical Center – University of Freiburg, Faculty of Medicine, University of Freiburg, Freiburg, Germany. [10]These authors contributed equally: Joy Edwards-Hicks, Petya Apostolova. ✉e-mail: epearce6@jhmi.edu

Methods

Mice

C57BL/6J (RRID: IMSR_JAX:000664), major histocompatibility complex (MHC) class I-restricted OVA-specific TCR OT-I transgenic mice (RRID: IMSR_JAX:003831) and CD45.1$^+$ C57BL/6J (B6.SJL-*Ptprc*^{a} *Pepc*^{b}/BoyJ; Jax, 002014) mouse strains were purchased from The Jackson Laboratory. Male and female mice (8–12 weeks old, age-matched and sex-matched between experimental conditions) were used in all experiments. All mice were maintained in the animal facilities at the Max Planck Institute for Immunobiology and Epigenetics or at the Johns Hopkins University under specific-pathogen-free conditions and following institutional animal use and care guidelines. Mice were exposed to a 14-h/10-h light/dark cycle and fed ad libitum (Ssniff, V1185-300 or Envigo 2018SX) with acidified water (pH 2.5–3.3). The room temperature and humidity were maintained and monitored. The animal protocols were approved by the Federal Ministry for Nature, Environment and Consumer Protection of the state of Baden-Württemberg, Germany and by the Johns Hopkins University Animal Care and Use (G-16/129, G-17/71 and MO19M71, MO22M15).

Primary T cell cultures

CD8$^+$ T cells were isolated from the spleens and lymph nodes of 8- to 12-week-old age-matched and sex-matched C57BL/6 mice using the EasySep CD8$^+$ T cell isolation kit (Stem Cell Technologies, 19753) according to the manufacturer's instructions. CD8$^+$ T cells were activated using plate-bound anti-CD3 (5 µg ml^{-1}; InVivoMab anti-mouse CD3, BioXCell, BE0002) and soluble anti-CD28 (0.5 µg ml^{-1}; InVivoMab anti-mouse CD28, BioXcell, BE0015) in 1640 media (Invitrogen) supplemented with 10% fetal calf serum (Gibco), 4 mM L-glutamine, 100 U ml^{-1} penicillin–streptomycin, 100 U ml^{-1} IL-2 (Peprotech), 55 µM beta-mercaptoethanol in a humidified incubator at 37 °C, atmospheric oxygen supplemented with 5% CO_2. Cells were stimulated for 48 h or 72 h as indicated in the figure, and then further expanded in IL-2 only. For the generation of T_M cells, IL-2 was replaced by 100 U ml^{-1} IL-15 starting from 72 h after activation for three d. Unstimulated cells were maintained as indicated in 100 U ml^{-1} IL-7 (Peprotech). For OT-I cultures, single-cell suspensions of splenocytes were stimulated for 48 h in IL-2-containing media as above in the presence of SIINFEKL peptide. At 48 h after activation, media was replaced with expansion media containing IL-2 only.

Cell lines

The mouse E.G7 lymphoblast cell line expressing OVA (EL4-OVA) was purchased from the American Type Culture Collection (ATCC no. CRL-2113; RRID: CVCL_3505). The mouse melanoma cell line B16-F10-OVA was a kind gift from D. Zehn (parental cell line B16-F10 from ATCC, CRL-6475). The human T lymphocyte cell Jurkat (ATCC, TIB-152) was a kind gift from J. Powell. Further authentication of the cell lines was not performed. Cells were maintained in 1640 medium (EL4-OVA and Jurkat) or DMEM (B16-F10-OVA) supplemented with 10% fetal calf serum, 4 mM L-glutamine, 100 U ml^{-1} penicillin–streptomycin and 55 µM beta-mercaptoethanol at 37 °C in a humidified incubator containing atmospheric oxygen supplemented with 5% CO_2. For EL4-OVA co-cultures, sub-confluent EL4-OVA cells were pre-stained with CellTrace Violet Cell Proliferation Kit (Invitrogen) and plated in fresh media at 50,000 cells per well in 100 µl.

L. monocytogenes infection studies

In total, 1×10^4 OT1$^+$ CD45.2$^+$ CD8$^+$ cells per mouse from donor splenocytes were transferred i.v. into congenic (CD45.1$^+$) age-matched recipient mice. After one d, mice were injected i.v. with a sublethal dose of 1×10^6 colony-forming units (CFUs) of recombinant *L. monocytogenes* expressing OVA deleted for *actA* (LmOVA Δ*actA*). On day four after infection, CD45.2$^+$ CD8$^+$ T cells were negatively isolated from recipient splenocytes using a BioLegend antibody cocktail comprising: CD11b (101204), CD11c (117304), CD19 (115504), CD45R (B220; 103204), CD49b (DX5) (108904), anti-MHC Class II (I-A/I-E) (107604), Ter-119 (116204), TCRγ/δ (118103), CD4 (100404) and CD45.1 (110704), all at a 600× dilution. Uninfected OT1$^+$ CD45.2$^+$ CD8$^+$ cells from donor splenocytes were used as a control. Lipids were extracted and analyzed by LC–QqQ–MS/MS. Flow cytometry analysis of the expansion of donor T cells was performed on day four and day seven after infection in peripheral blood.

Mouse melanoma model

Mice were shaved and 1×10^6 B16-F10-OVA cells in 100 µl were injected into the right flanks. For immunotherapy experiments, mice were randomized into two groups. On days three, six and nine after tumor inoculation, mice received intraperitoneal injections of either a combination of 0.2 mg per mouse of anti-CTLA-4 antibody (BioXCell, BE0032) and 0.2 mg per mouse of anti-PD-1 antibody (BioXCell, BE0146) or a combination of the respective IgG control antibodies (BioXCell, BE0091 and BE0089). The injection volume was 100 µl. Tumor sizes were measured with calipers every other day. The maximal allowed tumor size was 20 mm in diameter and animals were humanely euthanized if this size was reached. Mouse body condition was monitored over the whole experimental period. Mice were euthanized if the tumor diameter reached 20 mm or if there was tumor ulceration or bleeding. At the indicated time point, mice were humanely euthanized and the tumors were excised. Tumors were digested by shaking at 37 °C with 1 mg ml^{-1} collagenase IA (Sigma, C9891) and 50 µg ml^{-1} DNase I (Roche, 10104159001) for one h. Digested tumors were passed through a 70-µm filter then the lymphocyte fraction was obtained using a Percoll gradient. CD8$^+$ T cells were isolated by positive selection using CD8 TIL MicroBeads (Miltenyi Biotec, 130-116-478) according to the manufacturer's instructions.

For adoptive T cell transfer, 1×10^6 B16-F10-OVA cells in 100 µl were injected into the right flanks of mice. Tumor sizes were measured with calipers every other day. On day five after tumor inoculation, mice received an i.v. injection of 5×10^6 CTRL or CDIPT$^-$ OT-I T cells that had been activated for three d in vitro with the SIINFEKL peptide in the presence of IL-2. Tumor growth was measured until day 15. For analysis of TIL composition, the mice were euthanized when tumors reached 10 mm in diameter, the tumors were excised and digested as described above and TILs were analyzed by flow cytometry.

For lipidome analysis of TILs, mice were injected with 1×10^6 B16-F10-OVA cells in 100 µl into the right flanks. Tumors were measured until they reached seven mm in diameter, and were then excised and digested as described above. CD8$^+$ T cells were isolated by positive selection using CD8 TIL MicroBeads according to the manufacturer's instructions. CD8$^+$ T cells enriched from the spleens of the same mice were used as a control.

Human T cell analysis

Buffy coats for in vitro CD8$^+$ T cell experiments were kindly provided by the Institute for Transfusion Medicine and Gene Therapy, Medical Center – University of Freiburg (donor consent, anonymized), and processed as described below.

Human melanoma study

All procedures involving human participants were approved by the Ethics Committee of the Medical Center – University of Freiburg (protocol no. 310/18) and were conducted according to the Declaration of Helsinki. The study was registered at the German Clinical Trial Register (DRKS00023625). Adults with histologically confirmed malignant melanoma stage III or IV (male and female, $n = 13$, median age 55 years) were recruited with a standardized procedure based on assessment of inclusion and exclusion criteria. Inclusion criteria were a histologically confirmed malignant melanoma, no previous treatment with an immune checkpoint inhibitor and age >18 years. Participants with a previously diagnosed immunodeficiency syndrome were excluded. Study participants gave their written informed consent before study

enrollment. Collection of biological material was performed at the Department of Dermatology, Medical Center – University of Freiburg. No financial compensation was provided to participants. Peripheral blood mononuclear cells (PBMCs) were collected at two time points. The first time point was on the day of immune checkpoint inhibitor treatment initiation. The second time point was when the participant presented for the second administration of treatment. All samples were de-identified and analyzed in a pseudonymized manner. Disease response to checkpoint inhibitor treatment was assessed on a regular basis by ^{18}F positron emission tomography combined with computer tomography, computer tomography alone and/or magnetic resonance imaging. Responders were defined as participants who reached a partial or complete remission according to the radiologist's assessment. Partial remission was defined as a decrease in size and tumor metabolism of the majority of lesions. Complete remission was defined as the absence of malignant lesions. One participant was not eligible for response assessment. The median follow-up time was 318 d (range 184–484 d). Information on demographic characteristics and disease course was provided by the medical records at the Medical Center – University of Freiburg (Supplementary Table 1). Blood was collected in EDTA-coated tubes and stored at 4 °C before processing. Processing was performed within three h of blood collection. Blood was diluted at a 1:1 ratio with PBS containing 2% FCS and 1 mM EDTA. PBMCs were isolated using a density gradient method. Lymphoprep solution (Stem Cell) was pipetted to the bottom of SepMate-50 tubes (Stem Cell), and diluted blood carefully layered on top. After 10 min of centrifugation at 1,200*g*, the upper phase containing mononuclear cells was transferred to a new tube. PBMCs were washed twice with PBS with 2% FCS and 1 mM EDTA. Isolation of CD8$^+$ T cells was performed using the EasySep Human CD8$^+$ T Cell Isolation Kit (Stem Cell Technologies, 17953) according to the manufacturer's instructions.

Human Epstein–Barr virus study

Participants (male and female, $n = 3$, age unknown) with acute EBV infection were recruited based on clinical symptoms and positivity for EBV-VCA-IgM. All participants gave informed consent. The study was conducted according to the Declaration of Helsinki and approved by Ethics Committees of the University of Freiburg (protocol no. 282/11). No financial compensation was provided to participants. Circulating CD8$^+$ T cells were enriched and processed as described above.

CRISPR knockout studies

Primary mouse CD8$^+$ T cells were electroporated with gRNA-Cas9 ribonucleoproteins (RNPs) using the Amaxa 4D-Nucleofector system (Lonza). RNPs were prepared by complexing 180 pmol of gRNAs (IDT) with 60 pmol of Cas9 nuclease (IDT). Electroporation was performed in P4 Primary Cell solution using the program DS137. The nucleotide sequences for gRNA are listed in Supplementary Table 2.

Western blot analysis

For western blot analysis, cells were washed with ice-cold PBS and lysed in lysis buffer (Cell Signaling Technology) supplemented with 1 mM phenylmethyl sulfonyl fluoride (PMSF). Samples were frozen and thawed three times, followed by centrifugation at 20,000*g* for 10 min at 4 °C. Cleared protein lysate was denatured with LDS loading buffer for 10 min at 70 °C and loaded on precast 4–12% Bis–Tris protein gels (Life Technologies). Proteins were transferred onto nitrocellulose membranes using the iBLOT 2 system (Life Technologies) according to the manufacturer's protocols. Membranes were blocked with 5% wt/vol milk or BSA and 0.1% Tween-20 in TBS and incubated with the appropriate antibodies in 5% wt/vol BSA in TBS with 0.1% Tween-20 at 4 °C overnight. The antibodies were from Cell Signaling and used at a dilution of 1:1,000 unless otherwise stated: PLCγ1 (2822), Phospho-PLCγ1 (Tyr783) (2821), Phospho-c-Raf (Ser338) (Clone 56A6, 9427), Phospho-MEK1/2 (Ser217/221) (Clone 41G9, 9154), MEK1/2 (4694), Phospho-p44/42 MAPK (Erk1/2) (Thr202/Tyr204) (Clone D13.14.4E, 4370), p44/42 MAPK (Erk1/2) (Clone L34F12, 4696), α-tubulin (2125S; 1:5,000 dilution), β-actin (Clone 13E5, 4970S), ZAP70 (Clone 99F2, 2705 S), Phospho-Akt (Thr308; clone D25E6, 13038S), Phospho-Akt (Ser743) (clone D9E, 4060S), Akt (4685S) and PIS1 (Santa Cruz, sc-514255). All primary antibody incubations were followed by incubation with secondary horseradish peroxidase-conjugated antibody (goat anti-rabbit IgG, 31460 or goat anti-mouse IgG, 31430, Pierce/Thermo Scientific) in 5% milk or BSA and 0.1% Tween-20 in TBS (1:5,000–1:20,000 dilution) and visualized on radiosensitive film (Amersham) or a ChemiDoc imaging system (Bio-Rad) using chemiluminescent substrate (SuperSignal West Pico or Femto, Pierce).

Flow cytometry

Extracellular staining was performed in 2% FBS/PBS for 30 min on ice, and dead cells were excluded with the LIVE/DEAD Fixable Dead Cell Stain Kit (Thermo Fisher Scientific). For intracellular cytokine staining, cells were reactivated with PMA (50 ng ml^{-1}; Sigma) and ionomycin (500 ng ml^{-1}; Sigma) in the presence of brefeldin A (0.1%; BioLegend) for five h before fixation using Cytofix Cytoperm (BD Biosciences). For the co-culture experiments, brefeldin A was added directly into the co-culture (without extra restimulation) five h before staining. For intracellular p-ERK1/2, p-PLCγ1 and phalloidin (Thermo Fisher Scientific, A22287) staining, cells were fixed using Cytofix Cytoperm (BD Biosciences) before incubation with the antibody for 30 min. For intracellular p-MEK1 staining, cells were fixed with the Phosphoflow Fix Buffer I (BD Biosciences), followed by permeabilization with Phosphoflow Perm/Wash Buffer I (BD Biosciences). The following fluorochrome-conjugated monoclonal antibodies were used (dilution 1:200 unless otherwise specified): For surface staining of mouse cells: anti-CD8α (clone 53-6.7, BioLegend, 100706, 100712, 100713, 100714, 100738), anti-CD45.1 (clone A20, eBioscience, 25-0453-82), anti-CD45.2 (clone 104, BD, 553772), anti-CD127 (clone A7R34, BioLegend, 135020), anti-KLRG1 (clone MAFA, BioLegend, 138418), anti-CD44 (clone IM7, BioLegend, 103027, 103056), anti-CD62L (clone MEL-14, BioLegend, 104407, 104438), anti-CD25 (clone 3C7, BioLegend, 101907 and clone PC61, BioLegend, 102008), anti-PD-1 (clone RMP1-30, BioLegend, 109110 and clone 29F.1A12, BioLegend, 109110) and anti-CD69 (clone H1.2F3, BioLegend, 104512); for surface staining of human cells: anti-CD4-APC-Cy7 (clone RPA-T4, BioLegend, 300518), anti-CD8-KrO (clone B9.11, Beckman Coulter, B00067), anti-HLA-DR (clone G46-6, eBioscience, 556643); for intracellular staining of mouse cells: anti-IFN-γ (clone XMG1.2, BioLegend, 505808, 505810 and 505806), anti-Granzyme B (clone GB11, BioLegend, 515406 and clone NZGB, eBioscience, 12-8898-82), anti-phospho-PLCγ1 (clone A17025A, BioLegend, 612403, dilution 1:25), anti-phospho-ERK1/2 (clone 6B8B69, BioLegend, 369506), anti-phospho-MEK1 (clone A16117B, BioLegend, 610608, dilution 1:25); for intracellular staining of human cells: anti-Ki67 (clone MIB-1, Agilent Dako, F726801-8).

EdU incorporation was measured using the Click-iT EdU Alexa Fluor 647 Flow Cytometry Assay kit according to the provided instructions (Thermo Fisher Scientific, C10424). Cell proliferation was quantified using the CellTrace Violet Cell Proliferation kit for flow cytometry (Thermo Fisher Scientific, 34557). Flow cytometry analyses were performed on an LSRFortessa flow cytometer, FACSymphony and FACSCelesta flow cytometer (BD Biosciences) or CytoFLEX platform (Beckmann Coulter) and data were analyzed with FlowJo 10 software (BD Biosciences).

Analysis of membrane lipid order and lipid rafts

Cultured T_{eff} cells or Jurkat cells were first stained with the LIVE/DEAD Fixable Dead Cell Stain Kit (Thermo Fisher Scientific), followed by incubation with 5 μM di-4-ANEPPDHQ (Thermo Fisher Scientific, D36802) for 30 min in the dark at 37 °C, 5% CO_2. Flow cytometry analysis was

performed on a FACSymphony flow cytometer (BD Biosciences) immediately without washing or fixing the cells. High-order cells emit at ~570 nm and low-order cells emit at ~630 nm, allowing the gating of two separate populations. The GP value was calculated as a quantitative measure for lipid order as previously described[28]:

$$\mathrm{GP} = \frac{I(570\,nm) - I(630\,nm)}{I(570\,nm) + I(630\,nm)},\ I = \text{geometric mean fluorescence intensity}$$

Lipid rafts were quantified by measuring fluorescently labeled cholera toxin B subunit (CTB), which binds to glycosphingolipid GM1, an abundant component of lipid rafts. Cultured T_{eff} cells or Jurkat cells were first stained with the LIVE/DEAD Fixable Dead Cell Stain Kit (Thermo Fisher Scientific), followed by incubation with 25 μg ml^{-1} Alexa Fluor 488-conjugated recombinant Cholera Toxin Subunit B (Thermo Fisher Scientific, C34775) for 30 min in the dark at 4 °C. Cells were washed twice with staining buffer before flow cytometry acquisition.

Cytolysis assay
OT-I splenocytes were stimulated with plate-bound anti-CD3 (5 μg ml^{-1}) (InVivoMab anti-mouse CD3, BioXCell, BE0002), soluble anti-CD28 (0.5 μg ml^{-1}; InVivoMab anti-mouse CD28, BioXcell, BE0015) and 100 U ml^{-1} IL-2 (Peprotech) for 48 h, then cultured for a further 24 h in IL-2 plus vehicle or CDIPTi. OT-I cells were then washed and plated with CellTrace Violet pre-stained EL4-OVA cells over a dilution series. The percentage of dead EL4-OVA cells was determined after 8 h by flow cytometry. For assessment of cytokine production by OT-I T cells, Brefeldin A was added for the final 5 h of co-culture.

Pharmacological inhibitors
Inostamycin (CDIPTi) was a kind gift of M. Imoto and E. Tashiro[21]. Inostamycin was dissolved at a concentration of 1 mg ml^{-1} in methanol and used in cell culture at the indicated concentrations. Next, 2-DG (Sigma, L07338.14) was used in cell culture at 5 mM. KA (Cayman Chemical, 14079) was used in cell culture at 5 μM, and A939572 (SCDi) was used in cell culture at 100 nM (Sigma, SML2356).

Phospholipase C activity assay
PLC activity was measured using a colorimetric assay kit (Abcam, ab273343) according to the manufacturer's instructions. In total, 2×10^6 primary T_{eff} cells or Jurkat cells were used per sample. Data were collected on a SpectraMax M3 instrument with the SoftaMax Pro 7.1.2 software.

Calcium measurement
Basal calcium was measured using the Indo-1 AM dye according to the manufacturer's instructions (Thermo, I1223). In brief, cells were pelleted and resuspended in RPMI 1640 with 0.25 mM Indo-1 AM for 30 min at 37 °C. Cells were then washed and acquired by flow cytometry using the following parameters: unbound = 530/30, bound = 405/20. The bound/unbound ratio was calculated as a measure of basal calcium.

Organelle enrichment for lipidomic analysis
$CD8^+$ T cells were isolated and activated as described above for 96 h. Samples of 20×10^6 cells per organelle compartment were harvested. Organelle enrichment was performed using the following kits from Invent Biotechnologies according to the manufacturer's manuals: Minute Total Lipid Raft Isolation Kit for Mammalian Cells and Tissues (LR-039), Minute Mitochondria Isolation Kit for Mammalian Cells and Tissues (MP-007), Minute Lysosome Isolation Kit for Mammalian Cells/Tissues (LY-034), Minute Endosome Isolation and Cell Fractionation Kit (ED-028), Minute Golgi Apparatus Enrichment kit (GO-037), Minute ER Enrichment kit (ER-036) and Minute Cytoplasmic & Nuclear Extraction Kit for Cells (SC-003). Lipid extraction and PIP_n measurement were performed as described below.

Stable isotope labeling studies
To measure the contribution of U-^{13}C-glucose-derived carbon into PI synthesis, RPMI 1640 media (supplemented as above) was changed for RPMI 1640 no glucose media (supplemented as above) containing the indicated concentration of U-^{13}C-glucose or unlabeled glucose for 6 h or 24 h as indicated.

Preparation of lipids for cell culture
Soy-derived PI (Avanti, 840044P), 18:0-20:4 PI (Avanti, 850144) and LA (Sigma, L1376) were dissolved at a final concentration of 10 mM in 20:9:1 (vol/vol/vol) chloroform:methanol:water. One hundred μl of dissolved lipid was dried per 2-ml glass vial using a Genevac EZ2 speed vac and stored at −20 °C until the day of use. Fatty-acid-free BSA (Roche, 3117057001) was dissolved in RPMI 1640 at 10 mg ml^{-1} (10 min, 37 °C), and then conjugated to PI or LA (1 h, 37 °C). BSA-conjugated PI was used in cell culture at a final concentration of 100 μM (1 mg ml^{-1} BSA). OA was purchased pre-conjugated to BSA and used at a final concentration of 100 μM (Sigma, 03008).

Lipid extraction
In general, lipids were extracted using a biphasic Methyl *tert*-butyl ether (MTBE) extraction protocol (adapted from Matyash et al.[55]). In brief, cells were resuspended in 100 μl cold PBS in 8-ml glass vials. Cold methanol (750 μl), MTBE (2 ml) and water (625 μl) were added sequentially with vortexing. Samples were centrifuged to separate phases, and the upper organic phase was taken into a 2-ml glass vial using a glass stripette. Samples were dried using a Genevac EZ2 speed vac. Dried samples were stored at 4 °C, then resuspended in 50 μl 2:1:1 (vol/vol) 2-propanol:acetonitrile:water and transferred to a sample vial with conical glass insert before analysis.

For measurements of glycosphingolipids, lipid extraction was performed with a Folch extraction protocol adapted from ref. [56]. Briefly, cells were resuspended in 150 μl water, followed by addition of 400 μl methanol and 200 μl chloroform. Cells were then sonicated and after a centrifugation step, the clear supernatant was further processed. Phase separation was performed by addition of 100 μl 0.1 M KCl and the water/methanol-rich upper layer containing glycosphingolipids was collected. Solid phase extraction was performed using Bond Elut C8 cartridges (Agilent). Samples were dried using a Genevac EZ2 speed vac. Dried samples were stored at 4 °C, then resuspended in 50 μL 2:1:1 (vol/vol) 2-propanol:acetonitrile:water and transferred to a sample vial with conical glass insert before analysis.

Phosphatidylinositol phosphate extraction
PI phosphates were extracted and derivatized as described by Clark et al.[57]. In brief, cells were resuspended in 150 μl cold PBS in 2-ml tubes and quenched with 750 μl quench mixture (484 ml methanol, 242 ml $CHCl_3$ and 23.55 ml 1 M HCl). Phases were separated by adding 725 μl $CHCl_3$ and 170 μl 2 M HCl, and centrifuging at 12,500*g* for two min. The lower phase was collected and washed with 700 μl pre-derivatization wash (240 ml $CHCl_3$, 120 ml methanol and 90 ml 0.01 M HCl). Samples were centrifuged at 12,500*g* for two min and the lower phase was collected. Extracts were derivatized by adding 50 μl 2 M TMS-diazomethane in hexane for 10 min at room temperature, before quenching with 6 μl glacial acetic acid. Samples were washed twice with 700 μl post-derivatization wash (240 ml $CHCl_3$, 120 ml methanol and 90 ml H_2O), and the lower phase was collected in a 2-ml glass vial. Then, 100 μl 9:1 (vol/vol) methanol:water was added to each sample before drying under a stream of nitrogen gas. Just before the sample was completely dry, extracts were resuspended in 50 μl 9:1 (vol/vol) methanol:water ready for acquisition by LC–QqQ–MS/MS.

Lipid measurement by LC–MS/MS
Chromatographic separation was performed on an Agilent 1290 infinity II UHPLC system using an Agilent Zorbax Eclipse Plus C18 column

(100 × 2 mm, 1.8-µm particles). Buffer A was 10 mM ammonium formate in 60:40 acetonitrile:water. Buffer B was 10 mM ammonium formate in 90:10 2-propanol:acetonitrile. The gradient profile was: 0 min, 30% B, 0.2 ml min^{-1}; 0.5 min, 30% B, 0.25 ml min^{-1}; 0.6 min, 30% B, 0.4 ml min^{-1}; 1.2 min, 30% B, 0.4 ml min^{-1}; 5.2 min, 68% B, 0.4 ml min^{-1}; 21.2 min, 75% B, 0.4 ml min^{-1}; 21.7 min, 97% B, 0.4 ml min^{-1}; 26.0 min, 97% B, 0.4 ml min^{-1}; 26.5 min, 30% B, 0.4 ml min^{-1}; stop time, 28 min. Column temperature was 35 °C and autosamper temperature was 5 °C.

For LC–QqQ–MS/MS analysis, the LC system was coupled to an Agilent 6495 Triple Quad QQQ-MS. Data were acquired with the MassHunter LC/MS Data Acquisition Software (Agilent, version B.08.02). Lipids were identified by fragmentation and retention time (as predetermined by standards for each subclass), and peak area was determined using Agilent Mass Hunter software. To determine the concentration of PI, peak areas were normalized to the peak area of PI 8:0/8:0 (Avanti, 850181 P) that was added to samples before extraction.

For LC–QTOF–MS analysis, the LC system was coupled to a Bruker impact II QTOF MS or a Bruker timsTOF MS equipped with an ionBooster ESI source. The mass spectrometer was operated in negative mode without Auto MS/MS. The mass axis was calibrated at the beginning of every sample run. Data were acquired with the Compass Hystar software (Bruker, version 5.1.8.2). Lipids were identified by accurate mass, isotope distribution and by matching retention time to LC–QqQ–MS/MS data. Lipid peak areas were determined using the R package AssayR[58] or the software Metaboscape and TASQ (Bruker).

Phosphatidylinositol phosphate measurement by LC–MS

Targeted quantification of derivatized PIP_2 and PIP_3 species was carried out using an Agilent 1290 Infinity II UHPLC in line with an Agilent 6495 QQQ-MS operated in MRM mode. MRM settings were optimized for a pure standard of PIP_2 16:10/16:0 and propagated to other PIP_2 and PIP_3 species in accordance with the transitions described by Clark et al.[57]. LC separation was on a Waters BSH C4 column (100 × 2 mm, 1.7-µm particles) using a solvent gradient of 40% buffer A (0.1% formic acid in milliQ-H_2O) to 100% buffer B (0.1% formic acid in acetonitrile). The flow rate was 400 µl min^{-1}, autosampler temperature was 5 °C and injection volume was 10 µl. Data processing was performed using Agilent MassHunter software.

Phosphoinositide conversion assay

For the PI conversion assay, 16:0-18:1 PI(4)P and 18:0-20:4 PI(4) were purchased from Avanti and liposomes were produced by mixing 85 mol % 1-palmitoyl-2-oleoyl-glycero-3-phosphocholine (POPC), 10 mol % phosphatidylserine (POPS) with 5 mol % of the respective PI together with 0.1% Atto647N-DOPE or NBD-DPPE. The mixtures were evaporated under nitrogen flow and dried overnight in a vacuum. Dried lipids were resuspended in buffer containing 20 mM HEPES, 150 mM NaCl and 0.5 mM TCEP at 37 °C and subjected to six cycles of freeze thawing in liquid nitrogen. Liposomes were extruded to 100 nm and aliquoted, frozen in liquid nitrogen and stored at −20 °C. Membrane-coated beads were generated by mixing liposomes and 10-µm silica beads (Whitehouse Scientific) in 200 mM NaCl. Beads were washed twice with 20 mM HEPES and resuspended in buffer containing 20 mM HEPES, 150 mM NaCl and 0.5 mM TCEP.

Phosphoinositide conversion assay was carried out as previously described[29]. Membrane-coated beads were washed into 100 µl kinase buffer (20 mM HEPES (pH 7.0), 150 mM NaCl, 5 mM $MgCl_2$, 0.5 mM EGTA, 200 µg ml^{-1} β-casein, 20 mM BME and 20 mM glucose) in the presence of 1 mM ATP. Samples were applied to an imaging chamber and purified PLCδ-PH fused to RFP was added to a final concentration of 150 nM. Immediately before acquisition, reconstituted PIP5K1C was added to the beads at a final concentration of 50 nM. The reaction was monitored using a Leica SP8 Confocal Microscope with a Leica HC PL APO CS2 ×63/1.40 oil-immersion objective at 0.75 base zoom with 1,024 × 1,024-pixel scan at 3.4 s per frame. PLCδ-PH fused to RFP was purified from BL21 cells (CMC0014, Scientific Laboratory Supplies-reagents) and PIP5K1C was purified from Sf9 insect cells (B82501, Thermo Fisher) as described in detail elsewhere[29]. Recruitment of PLCδ was determined by measuring the MFIs on the beads by segmentation of either the NBD or the Atto647N signal as mask using ImageJ.

Data collection

Data collection and analysis were not performed blind to the conditions of the experiments. For in vitro experiments, T cells were equally distributed into multi-well plates and the treatment condition was randomly applied. For in vivo animal experiments, no conscious biases were used to assign experimental groups. Mice were randomly assigned between groups and analyzed along age-matched and sex-matched controls. For human participants, the allocation to a certain group was based on the clinical condition that was used as an experimental model (for example, healthy donor versus participant with an acute EBV infection). The study of humans was observational and not interventional, so that no randomization to different treatment groups was possible/necessary. No data were excluded.

Statistics and normalization

No statistical methods were used to predetermine sample sizes but our sample sizes are similar to those reported in previous publications[35,44,59]. Statistical analysis was performed using Prism 9 software (GraphPad) unless otherwise indicated. Data distribution was assumed to be normal but this was not formally tested. Results are represented as the mean ± s.e.m. Comparisons of two groups were calculated using an unpaired two-tailed Student's *t*-test; when one group was used for normalization and thus all values in this group were equal (for example, 0 or 1), a one-sample *t*-test was applied. Comparisons of more than two groups were calculated using ordinary one-way ANOVA or two-way ANOVA with the indicated appropriate test for multiple comparisons. Comparisons of matched participant samples were calculated using a two-tailed Wilcoxon matched-pairs signed-rank test. The selection of sample size was based on extensive experience with metabolic and in vivo tumor immunology assays. Quantile normalization of lipidomic data was carried out in R using the R package 'preprocessCore' (ref. [60]). Statistical analysis of whole lipidomic datasets was carried out in R using a one-way ANOVA.

Reporting summary

Further information on research design is available in the Nature Portfolio Reporting Summary linked to this article.

Data availability

RNA sequencing data were accessed in the Gene Expression Omnibus under accession number GSE171245[59]. Source data are provided with this paper.

References

55. Matyash, V., Liebisch, G., Kurzchalia, T. V., Shevchenko, A. & Schwudke, D. Lipid extraction by methyl-tert-butyl ether for high-throughput lipidomics. *J. Lipid Res.* **49**, 1137–1146 (2008).
56. Wong, M., Xu, G., Park, D., Barboza, M. & Lebrilla, C. B. Intact glycosphingolipidomic analysis of the cell membrane during differentiation yields extensive glycan and lipid changes. *Sci. Rep.* **8**, 10993 (2018).
57. Clark, J. et al. Quantification of PtdInsP3 molecular species in cells and tissues by mass spectrometry. *Nat. Methods* **8**, 267–272 (2011).
58. Wills, J., Edwards-Hicks, J. & Finch, A. J. AssayR: a simple mass spectrometry software tool for targeted metabolic and stable isotope tracer analyses. *Anal. Chem.* **89**, 9616–9619 (2017).
59. O'Sullivan, D. et al. Fever supports $CD8^+$ effector T cell responses by promoting mitochondrial translation. *Proc. Natl Acad. Sci. USA* **118**, e2023752118 (2021).

60. Bolstad, B. *preprocessCore: a collection of pre-processing functions*. R package version 1.42.0. https://github.com/bmbolstad/preprocessCore

Acknowledgements

The authors thank A. Shaw and Z. Katz for insightful discussion. This work was supported by the Max Planck Society, the Leibniz Prize, and the National Institutes of Health R01AI156274 (to E.L.P.), two Bloomberg Distinguished Professorships (to E.L.P. and E.J.P.), a research grant from Bristol Myers Squibb, a Marie-Sklodowska-Curie actions Individual Fellowship (to F.B.), a Sir Henry Wellcome Fellowship (to D.J.P.), two Alexander von Humboldt Fellowships (to M.V. and M.C.) and the Deutsche Forschungsgemeinschaft (DFG, German Research Foundation)—project no 492259164 (to P.A.) and SFB-1479 project no. 441891347 (to R.Z.).

Author contributions

Conceptualization, project insight and data interpretation: J.E.-H., P.A. and E.L.P. Performing and analyzing experiments: J.E.-H., P.A., J.M.B., H.M., M.A.S., M.C., R.I.K., M.V., G.E.C., D.E.S., F.B., B.K., J.D.C., F.H., A.P., C.S.F., G.C., R.L.K., M.S., M.C., H.P., J.M., K.G., L.F., M.M. and L.Z. Provided advice, material and scientific ideas: M.E.M., F.W., D.A.R.-S., F.M., B.B., R.Z., D.J.P., D.O.S. and E.J.P. Manuscript writing: J.E.H., P.A. and E.L.P.

Competing interests

E.L.P. is an SAB member of ImmunoMet Therapeutics and E.L.P. and E.J.P are Founders and Scientific Advisors to Rheos Medicines. The other authors declare no competing interests.

Additional information

Extended data is available for this paper at https://doi.org/10.1038/s41590-023-01419-y.

Supplementary information The online version contains supplementary material available at https://doi.org/10.1038/s41590-023-01419-y.

Correspondence and requests for materials should be addressed to Erika L. Pearce.

Peer review information *Nature Immunology* thanks Michael Dustin and the other, anonymous, reviewer(s) for their contribution to the peer review of this work. Primary Handling Editor: N. Bernard, in collaboration with the *Nature Immunology* team.

https://doi.org/10.1038/s41590-023-01419-y

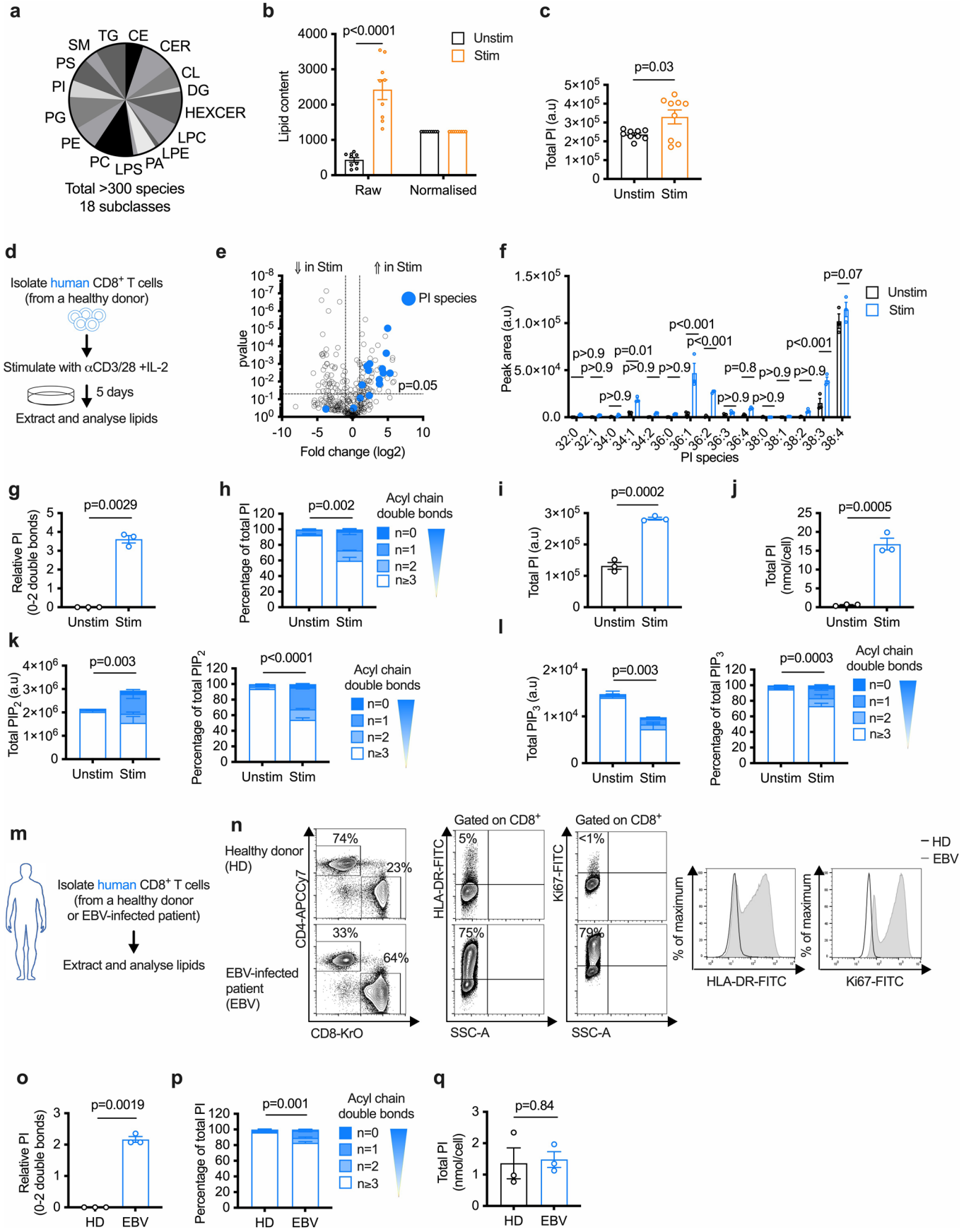

Extended Data Fig. 1 | See next page for caption.

https://doi.org/10.1038/s41590-023-01419-y

Extended Data Fig. 1 | Human CD8$^+$ T_E accumulate PIP_n with saturated acyl chains. **a**, Pie chart showing the number of lipid species measured by LC-QqQ-MS/MS in each of the 18 lipid subclasses. **b-c**, WT CD8$^+$ T cells were stimulated (Stim) with anti-CD3, anti-CD28 and IL-2 or cultured with IL-7 (unstim) for 3 days. **b**, Median lipid content per million cells before (raw) and after (normalized) quantile normalization is shown. n = 9 biologically independent samples across 3 independent experiments; unpaired two-tailed *t*-test. **c**, Relative total PI level calculated from quantile normalized lipid peak areas. n = 9 biologically independent samples across 3 independent experiments; unpaired two-tailed *t*-test. **d**, Experimental schematic. **e-f**, Volcano plot shows the log_2 fold change **(e)** or total PI **(f)** between Unstim and Stim conditions using quantile normalized lipid peak areas. n = 3 biologically independent samples; one-way ANOVA or two-way ANOVA corrected for multiple comparisons (Sidak test). **g**, Relative intensity of saturated PI normalized to Unstim (log_2 fold change). n = 3 biologically independent samples; one sample *t*-test. **h**, PI saturation percentage. n = 3 biologically independent samples; unpaired two-tailed *t*-test comparing saturated PI. **I**, Total PI. n = 3 biologically independent samples; unpaired two-tailed *t*-test. **j**, Total PI concentration (nmol/cell). n = 3 biologically independent samples; unpaired two-tailed *t*-test. **k**, Saturation of acyl chains in human T_E is expressed as a relative proportion of the total PIP_2 (left panel) and as a percentage of total PIP_2 (right panel). n = 5 biologically independent samples; unpaired two-tailed *t*-test comparing the total or percentage saturated PIP_2. Total polyunsaturated PIP_2 was not significantly different. **l**, Saturation of acyl chains in human T_E is expressed as a relative proportion of the total PIP_3 (left panel) and as a percentage of PIP_3 (right panel). n = 5 biologically independent samples; unpaired two-tailed *t*-test comparing the total or percentage saturated PIP_3. Total polyunsaturated PIP_3 was also significantly different ($p < 0.001$). **m**, Experimental schematic. **n**, Percentage CD8$^+$ cells, activation marker HLA-DR$^+$ cells, and proliferation marker Ki67$^+$ cells are shown. MFI of HLA-DR and Ki67 are also shown. **o**, Relative intensity of saturated PI normalized to HD (log_2 fold change). n = 3 HD and n = 3 EBV biologically independent samples; one sample *t*-test. **p**, PI saturation. n = 3 HD and n = 3 EBV biologically independent samples; unpaired two-tailed *t*-test comparing the summed percentage of saturated PI. **q**, Total PI concentration (nmol/cell). n = 3 HD and n = 3 EBV biologically independent samples; unpaired two-tailed *t*-test. Error bars show the standard error of the mean. a.u., arbitrary units.

https://doi.org/10.1038/s41590-023-01419-y

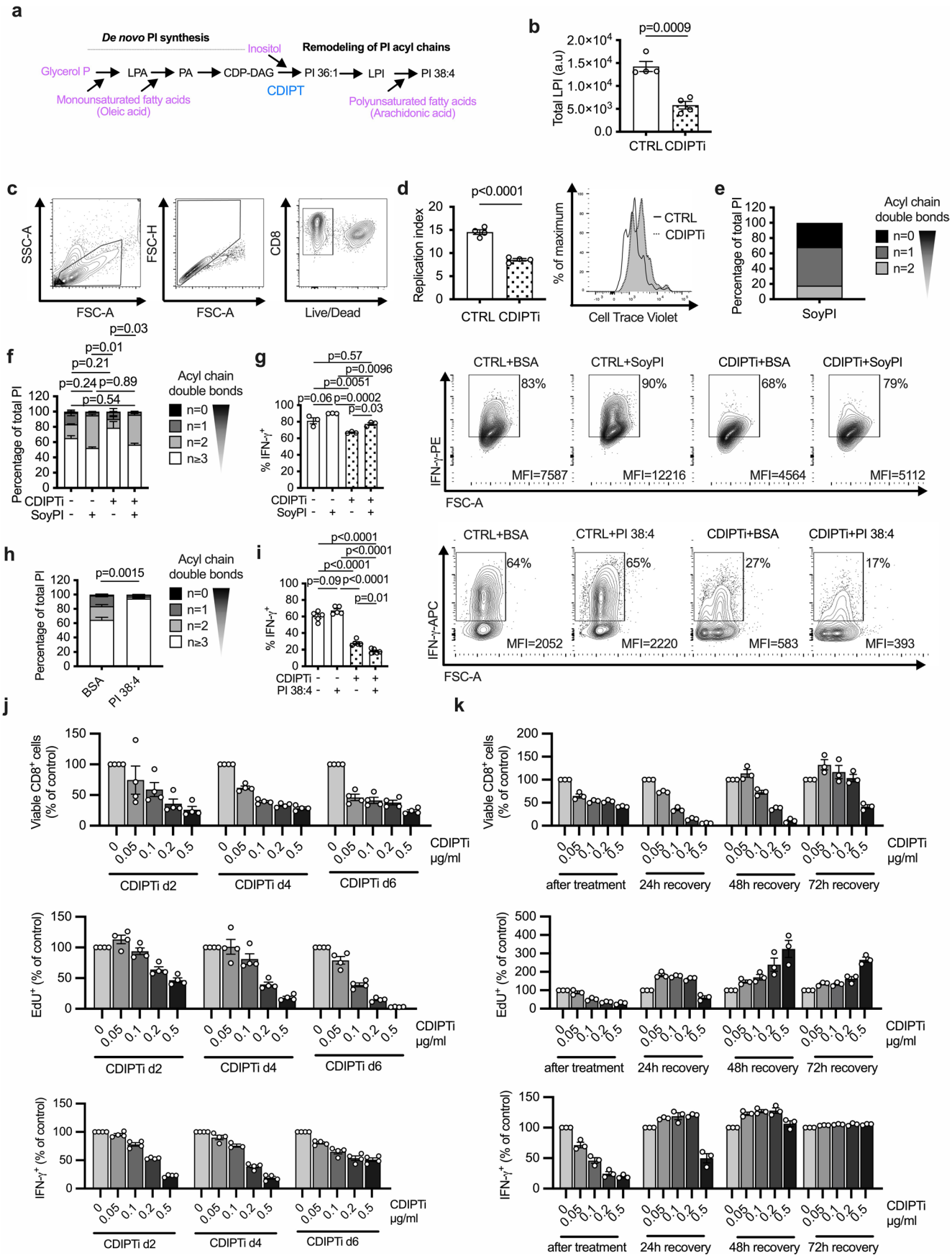

Extended Data Fig. 2 | See next page for caption.

https://doi.org/10.1038/s41590-023-01419-y

Extended Data Fig. 2 | CDIPT inhibition or deletion impairs T_E fitness and function. a, Simplified overview of PI *de novo* synthesis and remodeling. **b**, WT $CD8^+$ T cells were activated and treated as in Fig. 2a. Total lysophosphatidlyinositol (LPI) content is shown. n = 4 biologically independent samples; unpaired two-tailed *t*-test. **c**, Gating strategy for flow cytometry analysis. **d**, Replication Index based on cell trace violet dilution was calculated using FlowJo software. n = 4 biologically independent samples; unpaired two-tailed *t*-test. **e**, PI species present in PI derived from Soy expressed by degree of acyl chain saturation. **f-g**, Cells were prepared as in **(b)**, with the addition of BSA (10 mg/ml) control or BSA conjugated to Soy-derived PI (SoyPI, 100 µM) for the final day. **f**, Saturation of acyl chains expressed as a percentage of total PI. n = 3 biologically independent samples, one-way ANOVA corrected for multiple comparisons (Tukey test) comparing saturated PI. **g**, Percentage IFN-γ^+ cells are shown, gated on Live/Dead-aqua$^-$ and CD8-Brilliant Violet 421^+. n = 3 biologically independent samples; one-way ANOVA corrected for multiple comparisons (Tukey test). **h-I**, Cells were prepared as in **(b)**, with the addition of BSA (10 mg/ml) control or BSA conjugated to PI 38:4 (100 µM) for the final day. **h**, Saturation of acyl chains expressed as a percentage of total PI. n = 3 biologically independent samples; unpaired two-tailed *t*-test comparing saturated PI. **I**, Percentage IFN-γ^+ cells are shown, gated on Live/Dead-near-IR^- and CD8-Brilliant Violet 421^+. n = 5 biologically independent samples representative of three experiments; one-way ANOVA corrected for multiple comparisons (Tukey test). **j**, WT $CD8^+$ T cells were activated as in Fig. 2a and the CDIPT inhibitor inostamycin was added at the indicated concentrations for 24 h starting either after either two, four or six days of activation. Upper panel: percentage of viable $CD8^+$ cells. Cells were gated on FSC and SSC and single cells. Middle panel: percentage of EdU^+ cells. Cells were gated on Live/Dead-aqua$^-$ CD8-APC-$Cy7^+$. Lower panel: percentage of IFN-γ^+ cells. Cells were gated on Live/Dead-aqua$^-$ CD8-APC-$Cy7^+$. For each time point, the values were normalized to the values of the control samples (0 µg/ml CDIPTi). n = 4 biologically independent samples representative of two independent experiments. **k**, WT $CD8^+$ T cells were activated and treated as in Fig. 2a. After 24 h of CDIPTi treatment, the cells were cultured in media without CDIPTi for the indicated time intervals. Upper panel: percentage of viable $CD8^+$ cells. Cells were gated on FSC and SSC and single cells. Middle panel: percentage of EdU^+ cells. Cells were gated on Live/Dead-aqua$^-$ CD8-APC-$Cy7^+$. Lower panel: percentage of IFN-γ^+ cells. Cells were gated on Live/Dead-aqua$^-$ CD8-APC-$Cy7^+$. For each time point, the values were normalized to the values of the control samples at the respective time point (0 µg/ml CDIPTi). n = 3 biologically independent samples representative of two independent experiments. Error bars show s.e.m.

https://doi.org/10.1038/s41590-023-01419-y

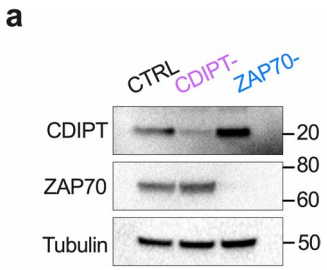

Extended Data Fig. 3 | CRISPR-Cas9 deletion efficiency for CDIPT and ZAP70. a, The efficiency of CRISPR-Cas9 for CDIPT and ZAP70 was verified by measuring protein expression.

https://doi.org/10.1038/s41590-023-01419-y

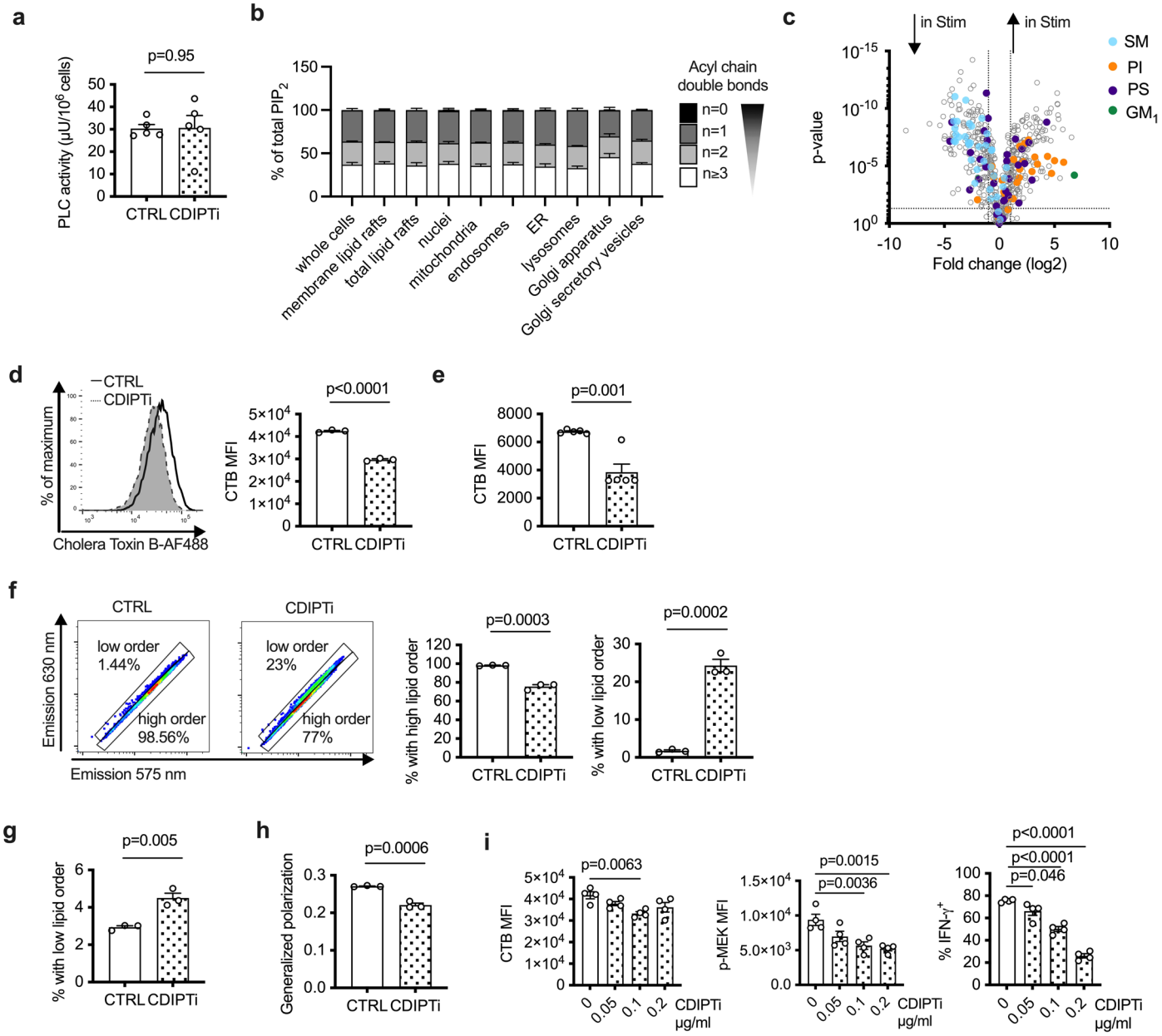

Extended Data Fig. 4 | Inhibition of CDIPT changes membrane lipid order and impairs lipid raft formation. a, Phospholipase C activity in Jurkat T cells cultured in the presence or absence of 0.5 μg/ml CDIPT inhibitor and activated for 30 min with 50 ng/ml PMA and 500 ng/ml ionomycin. n = 5 biologically independent samples representative of 2 independent experiments; unpaired two-tailed t-test. **b**, WT CD8$^+$ T cells were activated and cellular compartments were enriched as in Fig. 4i. Saturation of acyl chains expressed as a percentage of total PIP_2 across organelles. n = 4 biologically independent samples. **c**, WT CD8$^+$ T cells were isolated and activated or cultured in IL-7 as in Fig. 1a. Volcano plot shows the $\log_2$ fold change between Unstim and Stim using quantile normalized lipid peak areas. n = 5 biologically independent samples across 2 independent experiments; one-way ANOVA. Lipids from the following subclasses are highlighted: sphingomyelin (SM) in blue, phosphatidylinositol (PI) in orange, phosphatidylserine (PS) in purple and ganglioside GM1 in green. **d**, Cholera toxin subunit B measurement on primary CD8$^+$ T_E activated and treated as in Fig. 2a. n = 3 biologically independent samples representative of 3 independent experiments; unpaired two-tailed t-test. **e**, Cholera toxin subunit b measurement on Jurkat T cells treated as in **(a)**. n = 5 biologically independent samples representative of 2 independent experiments; unpaired two-tailed t-test. **f**, WT CD8$^+$ T cells were activated and treated as in Fig. 2a. Membrane lipid order was assessed by a di-4-ANEPPDHQ staining. Percentage of cells with high lipid order (di-4-ANEPPDHQ emission at 630 nm) and low lipid order (di-4-ANEPPDHQ emission at 570 nm). n = 3 biologically independent samples representative of 3 independent experiments; unpaired two-tailed t-test. **g**, Percentage of Jurkat T cells with low lipid order as determined by di-4-ANEPPDHQ flow cytometry staining after treatment as in **(a)**. n = 3 biologically independent samples representative of two independent experiments; unpaired two-tailed t-test. **(h)** Generalized polarization (GP) index as a normalized intensity ratio of the two spectral emissions for CD8$^+$ T_E analyzed as in **(e)**. n = 3 biologically independent samples representative of 3 independent experiments; unpaired two-tailed t-test. **(I)** WT CD8$^+$ T cells were activated and treated as in Fig. 2a except that the CDIPT inhibitor was used at the indicated concentrations. Cells were gated on Live/Dead-aqua$^-$ CD8-APC-Cy7$^+$. Left panel: Cholera toxin subunit B binding. Middle panel: mean fluorescence intensity of phosphorylated MEK1. Right panel: Percentage of IFN-γ$^+$ cells. n = 4 biologically independent samples representative of two independent experiments; one-way ANOVA with Dunnett's multiple comparisons test comparing all groups to '0 μg/ml'. Error bars show the standard error of the mean.

https://doi.org/10.1038/s41590-023-01419-y

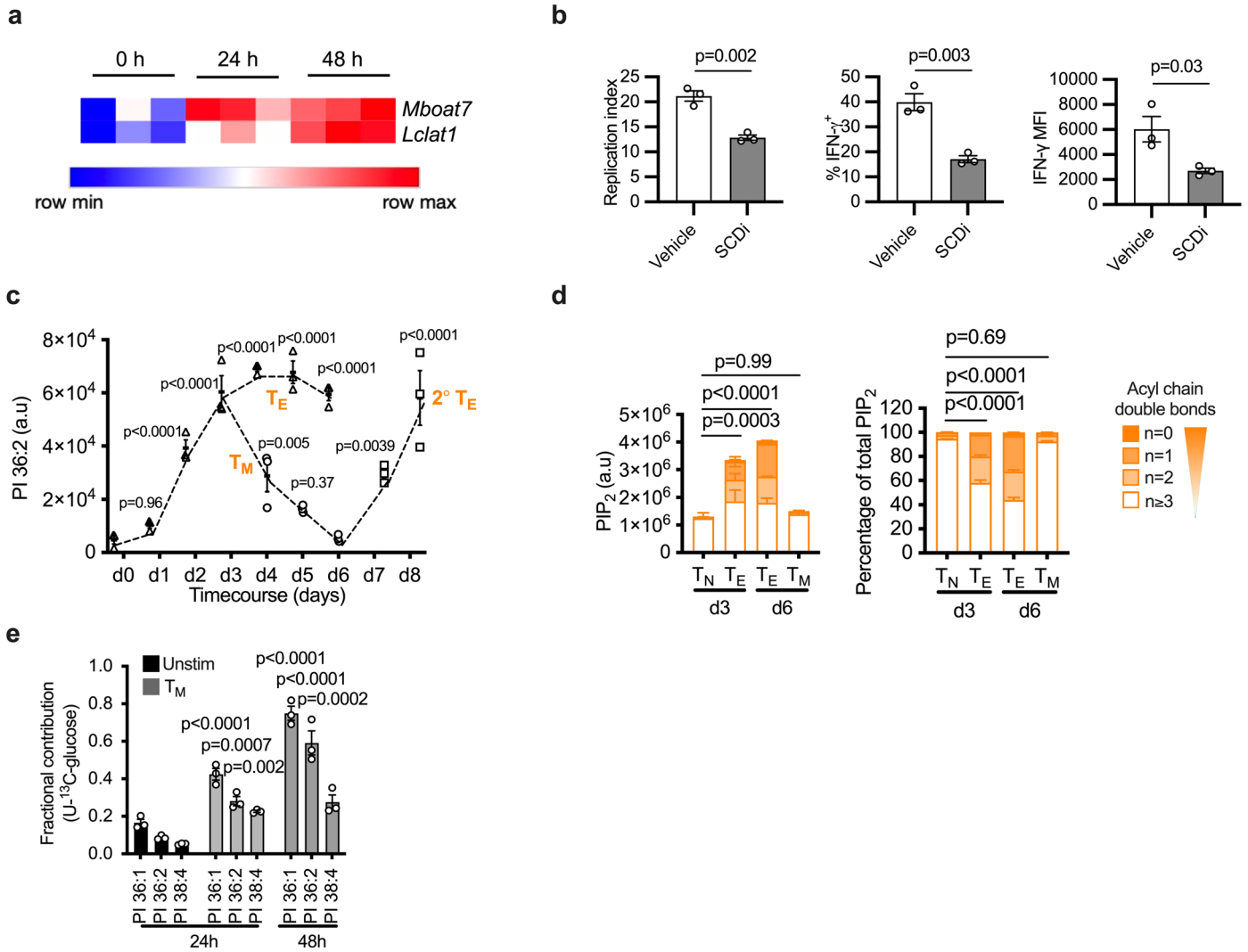

Extended Data Fig. 5 | T_E PIPn synthesis depends on glycolytic metabolism. **a**, WT CD8$^+$ T cells were isolated from spleens and lymph nodes of C57BL/6 mice then stimulated with plate-bound anti-CD3 (5 µg/ml), soluble anti-CD28 (0.5 µg/ml) and IL-2 (100 U/ml) for 2 days. Samples for RNA sequencing were harvested every 24 h. Heatmap depicting the gene expression levels of *Lclat1* and *Mboat7* in n = 3 biologically independent samples. **b**, WT CD8$^+$ T cells were isolated and activated as in **(a)**, followed by a treatment for 24 h with the Stearoyl-CoA-desaturase inhibitor A939572 (SCDi, 100 nM) in the presence of IL-2. Left panel: Replication Index based on Cell Trace Violet dilution calculated using FlowJo software. Middle and right panel: intracellular expression of IFN-γ. Cells were gated on Live/Dead-IR$^-$, CD8-APC$^+$. n = 3 biologically independent samples; unpaired two-tailed t-test. **c, d** WT CD8$^+$ T cells were isolated and activated as in **(a)**, followed by culture in IL-2 for 24 h. On d3, cells were either switched to IL-15 (100 U/ml, T_M) or maintained in IL-2 until d6. T_M were re-activated on d6 by stimulation with plate-bound anti-CD3 (5 µg/ml), soluble anti-CD28 (0.5 µg/ml) and IL-2 (100 U/ml) for 2 days to generate secondary T_E. **c**, Relative amount of PI 36:2 measured every 24 h. n = 3 biologically independent samples; one-way ANOVA corrected for multiple comparisons (Dunnett test) compared all groups to 0 h timepoint. **d**, Saturation of acyl chains expressed as a proportion of total PIP_2 (left panel) and as a percentage of PIP_2 (right panel). Statistical analysis of the saturated PI on n = 5 independent biological samples; one-way ANOVA with Dunnett's multiple comparisons's test compared all groups to 'Tn d3'. **e**, WT CD8$^+$ T cells were differentiated into T_M as in **(c)**, with the addition of 100% U-^{13}C-glucose 24 h before lipid analysis at each timepoint. Unstimulated cells were cultured in IL-7 with 100% U-^{13}C-glucose. Fractional contribution of ^{13}C-glucose-derived carbon to PI species was calculated. n = 3 biologically independent samples, two-way ANOVA with correction for multiple comparisons (Sidak's test) comparing PI species in each group with the relevant 24 h unstimulated PI. Error bars show the standard error of the mean.

https://doi.org/10.1038/s41590-023-01419-y

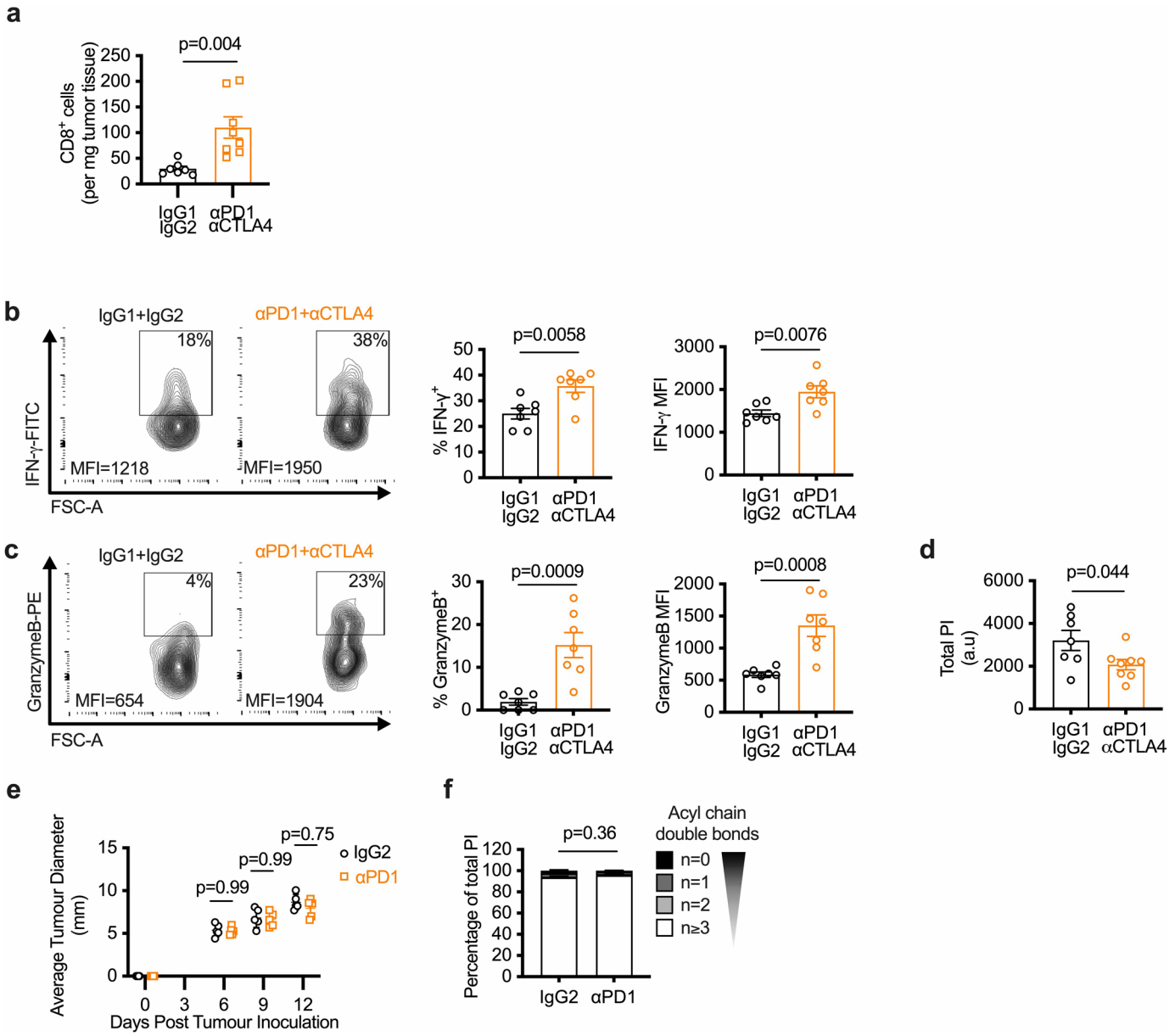

Extended Data Fig. 6 | Elevated numbers and cytokine production by CD8⁺ T cells after immunotherapy. a–d, Sex-matched C57BL/6 mice were injected in the right flank with 1×10^6 B16-F10-OVA cells. After 3 days, mice were given i.p. injections of anti-PD1 and anti-CTLA4 (aPD1 + aCTLA4) or matching isotype controls (IgG1 + IgG2) every 3 days for 3 rounds in total. Tumor growth was measured up to day 16 post-tumor injection and $CD8^+$ T cells were isolated on day 12 post-tumor injection to measure T cell function and lipid composition. **a**, $CD8^+$ tumor infiltrating lymphocytes (TILs) on day 12 post-tumor injection normalized to tumor weight. n = 7 IgG1 + IgG2 and n = 8 aPD1 + aCTLA4 biologically independent samples; unpaired two-tailed t-test. **b–c**, TILs were isolated day 12 post-tumor injection and restimulated with PMA/ionomycin plus brefeldin A for 5 h *in vitro*. n = 7 biologically independent samples per group, unpaired two-tailed t-test. **b**, Representative contour plots of IFN-γ expression (left panel), percentage IFN-γ^+ (middle panel) and IFN-γ expression (right panel) are shown. **c**, Representative contour plots of Granzyme B expression (left panel), percentage Granzyme B^+ (middle panel) and Granzyme B expression (right panel) are shown. **d**, Relative total PI calculated from quantile normalized lipid peak areas. n = 7 IgG1 + IgG2 and n = 8 aPD1 + aCTLA4 biologically independent samples; unpaired two-tailed t-test. **e-f**, Sex-matched C57BL/6 mice were injected in the right flank with $1x10^6$ B16-F10-OVA cells. After 3 days, mice were given i.p. injections of anti-PD1 antibody or matching isotype control (IgG2) every 3 days for 3 rounds in total. Tumor growth was measured up to day 12 post-tumor injection and $CD8^+$ T cells were isolated on day 12 post-tumor injection to measure T cell function and lipid composition. **e**, Average tumor diameter measured at the indicated time points. n = 5 biologically independent samples per group; two-way ANOVA corrected for multiple comparisons (Sidak test) comparing the two groups at each time point across the dataset. **f**, Lipids were analyzed from TILs on day 12 post-tumor injection. Saturation of acyl chains is expressed as a percentage of total PI. n = 5 biologically independent samples per group; unpaired two-tailed t-test comparing saturated PI. Error bars show the standard error of the mean.

nature portfolio

Corresponding author(s): Erika L. Pearce

Last updated by author(s): Nov 12, 2022

Reporting Summary

Nature Portfolio wishes to improve the reproducibility of the work that we publish. This form provides structure for consistency and transparency in reporting. For further information on Nature Portfolio policies, see our Editorial Policies and the Editorial Policy Checklist.

Statistics

For all statistical analyses, confirm that the following items are present in the figure legend, table legend, main text, or Methods section.

n/a	Confirmed	
☐	☒	The exact sample size (*n*) for each experimental group/condition, given as a discrete number and unit of measurement
☒	☐	A statement on whether measurements were taken from distinct samples or whether the same sample was measured repeatedly
☐	☒	The statistical test(s) used AND whether they are one- or two-sided *Only common tests should be described solely by name; describe more complex techniques in the Methods section.*
☒	☐	A description of all covariates tested
☐	☒	A description of any assumptions or corrections, such as tests of normality and adjustment for multiple comparisons
☐	☒	A full description of the statistical parameters including central tendency (e.g. means) or other basic estimates (e.g. regression coefficient) AND variation (e.g. standard deviation) or associated estimates of uncertainty (e.g. confidence intervals)
☐	☒	For null hypothesis testing, the test statistic (e.g. *F*, *t*, *r*) with confidence intervals, effect sizes, degrees of freedom and *P* value noted *Give P values as exact values whenever suitable.*
☒	☐	For Bayesian analysis, information on the choice of priors and Markov chain Monte Carlo settings
☒	☐	For hierarchical and complex designs, identification of the appropriate level for tests and full reporting of outcomes
☒	☐	Estimates of effect sizes (e.g. Cohen's *d*, Pearson's *r*), indicating how they were calculated

Our web collection on statistics for biologists contains articles on many of the points above.

Software and code

Policy information about availability of computer code

Data collection	Flow cytometry data were collected on a LSRFortessa, FACSymphony, FACSCelesta (all BD Bioscience) using the BD FACSDiva Software or CytoFLEX (Beckmann Coulter) flow cytometer. LC-MS data were collected using the MassHunter LC/MS Data Acquisition Software (Agilent, Version B.08.02) or Compass Hystar (Bruker, Version 5.1.8.2). Data from colorimetric assays were collected on a SpectraMax M3 instrument using the SoftaMax Pro 7.1.2 software. Western blot data was acquired using the Image Lab Touch software on a Chemidoc Imaging System (Biorad).
Data analysis	Flow cytometry data were analyzed with Flow Jo (BD Bioscience, V10.7.2). LC-MS data were analyzed with Metaboscape (Bruker, V2021-2022b), TASQ (Bruker, V2022), Mass Hunter Quantitative Analysis for QQQ (Agilent, Version B.08.00) or using the R package Assay R (Wills J et al, DOI: 10.1021/acs.analchem.7b02401). Data analysis for the phosphoinositide conversion assay was performed using ImageJ. Quantile normalization of lipidomic data was carried out in R using the R package "preprocessCore" (Bolstad B (2017) preprocessCore: A collection of pre-processing functions. R package version 1.40.0.). Statistical analysis was carried out using the Prism software (Graphpad, V8-9) or in R.

For manuscripts utilizing custom algorithms or software that are central to the research but not yet described in published literature, software must be made available to editors and reviewers. We strongly encourage code deposition in a community repository (e.g. GitHub). See the Nature Portfolio guidelines for submitting code & software for further information.

Data

Policy information about availability of data

All manuscripts must include a data availability statement. This statement should provide the following information, where applicable:

- Accession codes, unique identifiers, or web links for publicly available datasets
- A description of any restrictions on data availability
- For clinical datasets or third party data, please ensure that the statement adheres to our policy

RNA sequencing data were obtained from a previous study published by our group (Gene Expression Omnibus repository, https://www.ncbi.nlm.nih.gov/geo/, GEO accession number GSE171245, O'Sullivan et al.)

Field-specific reporting

Please select the one below that is the best fit for your research. If you are not sure, read the appropriate sections before making your selection.

☒ Life sciences ☐ Behavioural & social sciences ☐ Ecological, evolutionary & environmental sciences

For a reference copy of the document with all sections, see nature.com/documents/nr-reporting-summary-flat.pdf

Life sciences study design

All studies must disclose on these points even when the disclosure is negative.

Sample size	Sample size for animal experiments was calculated using professional advice and the statistical software G-power. Sample size for in vitro experiments was not predetermined using statistical methods. Sample sizes were determined based on the standard in the field. Replication between biological samples was robust and at least n=3 biological replicates were used for each experiment.
Data exclusions	No data were excluded throughout the manuscript.
Replication	Most experiments were repeated 3 times. Some experiments were repeated only twice or 1 time, in which cases, at least n=3 independent biological samples, partly pooled from multiple animals each, were used. All attempts at replication were successful.
Randomization	For in vitro experiments, T cells were equally distributed into multi-well plates and the treatment condition was randomly applied. For in vivo animal experiments, no conscious biases were used to assign experimental groups. Mice were randomly assigned between groups and analyzed along age- and sex-matched controls. For human participants, the allocation to a certain group was based on the clinical condition that was used as an experimental model (e.g. healthy donor vs. patient with an acute EBV infection). The study of human participants was observational and not interventional, so that no randomization to different treatment groups was possible/necessary.
Blinding	Blinding was not relevant in this study, as animal experiments used inbred genetically identical mice. All animals and in vitro samples were standardized and were treated in the exatly same way prior the application of the experimental treatment. All assessments were carried out using multiple independent replicates.

Reporting for specific materials, systems and methods

We require information from authors about some types of materials, experimental systems and methods used in many studies. Here, indicate whether each material, system or method listed is relevant to your study. If you are not sure if a list item applies to your research, read the appropriate section before selecting a response.

Materials & experimental systems

n/a	Involved in the study
☐	☒ Antibodies
☐	☒ Eukaryotic cell lines
☒	☐ Palaeontology and archaeology
☐	☒ Animals and other organisms
☐	☒ Human research participants
☒	☐ Clinical data
☒	☐ Dual use research of concern

Methods

n/a	Involved in the study
☒	☐ ChIP-seq
☐	☒ Flow cytometry
☒	☐ MRI-based neuroimaging

Antibodies

Antibodies used	The antibodies for western blot were from Cell Signaling and used at a dilution of 1:1,000 unless otherwise stated: PLCγ1 (Cat #2822), Phospho-PLCγ1 (Tyr783) (Cat #2821), Phospho-c-Raf (Ser338) (Clone 56A6, Cat #9427), Phospho-MEK1/2 (Clone 41G9, Ser217/221) (Cat #9154), MEK1/2 (Cat #4694), Phospho-p44/42 MAPK (Erk1/2) (Clone D13.14.4E, Thr202/Tyr204) (Cat #4370), p44/42 MAPK

(Erk1/2) (Clone L34F12, Cat #4696), Phospho-Akt (Thr308, Clone D25E6, Cat #13038S), Phospho-Akt (Ser473, Clone D9E, Cat #4060S), Akt (Cat #4685S) α-tubulin (Clone 11H10, Cat #2125S; 1:5,000), β-Actin (Clone 13E5, Cat #4970S), ZAP70 (Clone 99F2, Cat #2705S), and anti-PIS1 (Santa Cruz, Clone C-2, Cat #sc-514255).
The following HRP-conjugated antibodies were used as secondary antibodies for westen blot (dilution 1:5,000 - 1:20,000): Goat anti-rabbit IgG (H+L) Secondary antibody, HRP (Cat #31460, Pierce/ThermoScientific) and Goat anti-Mouse IgG (H+L) Secondary antibody. HRP (Cat #31430, Pierce/ThermoScientific).

The following fluorochrome-conjugated monoclonal antibodies were used for flow cytometry:
For surface staining of murine cells:
anti-CD8α (clone 53-6.7, Biolegend Cat #100706, 100712, 100713, 100714, 100738), anti-CD45.1 (clone A20, eBioscience Cat#25-0453-82), anti-CD45.2 (clone 104, BD Cat#553772), anti-CD127 (clone A7R34, Biolegend Cat#135020), anti-KLRG1 (clone MAFA, Biolegend Cat#138418), anti-CD44 (clone IM7, Biolegend Cat#103027, 103056), anti-CD62L (clone MEL-14, Biolegend Cat#104407, 104438), anti-CD25 (clone 3C7, Biolegend Cat#101907 and clone PC61, Biolegend Cat#102008), anti-PD-1 (clone RMP1-30, Biolegend Cat#109110 and clone 29F.1A12, Biolegend Cat#109110), and anti-CD69 (clone H1.2F3, Biolegend Cat#104512).
For surface staining of human cells: anti-CD4-APC-Cy7 (clone RPA-T4, Biolegend Cat#300518), anti-CD8-KrO (clone B9.11, Beckman Coulter Cat#B00067), anti-HLA-DR (clone G46-6, eBioscience Cat#556643).
For intracellular staining of murine cells: anti-IFNg (clone XMG1.2, Biolegend Cat#505808, 505810 and 505806), anti-Granzyme B (clone GB11, Biolegend Cat#515406 and clone NZGB, eBioscience Cat#12-8898-82), anti-phospho-PLCg1 (clone A17025A, Biolegend Cat#612403), anti-phospho-ERK1/2 (clone 6B8B69, Biolegend, Cat#369506), anti-phospho-MEK1 (clone A16117B, Biolegend Cat#610608).
For intracellular staining of human cells: anti-Ki67 (clone MIB-1, Agilent Dako Cat#F726801-8).

CD45.2+ CD8+ T cells were negatively isolated from recipient splenocytes using a Biolegend antibody cocktail comprising: CD11b (Cat# 101204), CD11c (Cat# 117304), CD19 (Cat# 115504), CD45R (B220) (Cat# 103204), CD49b (DX5) (Cat# 108904), Anti-MHC Class II (I-A/I-E) (Cat# 107604), Ter-119 (Cat# 116204), TCRγ/δ (Cat# 118103), CD4 (Cat# 100404), and CD45.1 (Cat# 110704). All antibodies were used in a 600X dilution of the originally provided concentration.

Following antibodies were used for in vivo treatment of mice (0.2 mg/mouse): anti-CTLA4(BioXCell, Cat #BE0032), anti-PD-1 (BioXCell, Cat #BE0146), polyclonal Armenian Hamster IgG (BioXCell, Cat #BE0091), rat IgG2a isotype control (BioXCell, Cat #BE0089).

Validation

All antibodies listed have been used in a number of previous publications, including our own. All antibodies are commercially available and have been validated by the manufacturers.
Anti-PLCγ1 Antibody (Cell Signaling Technology, Cat #2822): This antibody detects endogenous levels of total PLCγ1 protein and does not cross-react with PLCγ2. It has been validated in human, mouse and rat. Cited in more than 150 publications. https://www.cellsignal.com/products/primary-antibodies/plcg1-antibody/2822

Anti-Phospho-PLCγ1 (Tyr783) Antibody (Cell Signaling Technology, Cat #2821): This antibody detects PLCγ1 only when phosphorylated at tyrosine 783. It does not cross-react with phosphorylated PLCγ2 or other PLCs. It has been validated in human, mouse and rat. Cited in more than 250 publications. https://www.cellsignal.com/products/primary-antibodies/phospho-plcg1-tyr783-antibody/2821

Anti-Phospho-c-Raf (Ser338) (56A6) Rabbit monocloncal antibody (Cell Signaling Technology, Cat #9427): Phospho-c-Raf (Ser338) (56A6) Rabbit mAb detects endogenous levels of c-Raf only when phosphorylated at Ser338. It has been validated in Human, Mouse, Rat and Monkey. Cited in more than 200 publications. https://www.cellsignal.com/products/primary-antibodies/phospho-c-raf-ser338-56a6-rabbit-mab/9427

Anti-Phospho-MEK1/2 (Ser217/221) (41G9) Rabbit monoclonal antibody (Cell Signaling Technology, Cat #9154): This antibody detects endogenous levels of MEK1/2 only when activated by phosphorylation at Ser217/221. It has been validated in Human, Mouse, Rat and Monkey. Cited in more than 750 publications. https://www.cellsignal.com/products/primary-antibodies/phospho-mek1-2-ser217-221-41g9-rabbit-mab/9154

Anti-MEK1/2 (L38C12) Mouse mAb (Cell Signaling Technology, Cat #4694): This antibody detects endogenous levels of total MEK1/2 protein. It has been validated in Human, Mouse, Rat and Monkey. Cited in more than 250 publications. https://www.cellsignal.com/products/primary-antibodies/mek1-2-l38c12-mouse-mab/4694

Anti-Phospho-p44/42 MAPK (Erk1/2) (Thr202/Tyr204) (D13.14.4E) XP® Rabbit monoclonal antibody (Cell Signaling Technology, Cat #4370): This antibody detects endogenous levels of p44 and p42 MAP Kinase (Erk1 and Erk2) when dually phosphorylated at Thr202 and Tyr204 of Erk1 (Thr185 and Tyr187 of Erk2), and singly phosphorylated at Thr202. This antibody does not cross-react with the corresponding phosphorylated residues of either JNK/SAPK or p38 MAP kinases. It has been validated in Human, Mouse, Rat, Hamster, Monkey, Mink, D. melanogaster, Zebrafish, Bovine, Dog, Pig, S. cerevisiae. Cited in more than 8000 publications. https://www.cellsignal.com/products/primary-antibodies/phospho-p44-42-mapk-erk1-2-thr202-tyr204-d13-14-4e-xp-rabbit-mab/4370

Anti-p44/42 MAPK (Erk1/2) (L34F12) Mouse monoclonal antibody (Cell Signaling Technology, Cat #4696): This antibody detects endogenous levels of total p44/42 MAP kinase (Erk1/Erk2) protein. In some systems this antibody may recognize p42/Erk2 more readily than p44/Erk1. The antibody does not cross-react with JNK/SAPK or p38 MAP kinase. It has been validated in Human, Mouse, Rat, Monkey, Mink, Zebrafish, Bovine and Pig. Cited in more than 700 publications. https://www.cellsignal.com/products/primary-antibodies/p44-42-mapk-erk1-2-l34f12-mouse-mab/4696

Anti-Phospho-Akt (Thr308, D25E6) Rabbit monoclonal antibody (Cell Signaling Technology, Cat #13038S): This antibody recognizes endogenous levels of Akt1 protein only when phosphorylated at Thr308. This antibody also recognizes endogenous levels of Akt2 protein when phosphorylated at Thr309 or Akt3 protein when phosphorylated at Thr305. It has been validated in Human, Mouse, Rat and Monkey. Cited in more than 800 publications. https://www.cellsignal.com/products/primary-antibodies/phospho-akt-thr308-d25e6-xp-rabbit-mab/13038?site-search-type=Products&N=4294956287&Ntt=13038s&fromPage=plp&_requestid=2750985

Anti-Phospho-Akt (Ser473, D9E) Rabbit monoclonal antibody (Cell Signaling Technology, Cat #4060S): This antibody detects endogenous levels of Akt1 only when phosphorylated at Ser473. This antibody also recognizes Akt2 and Akt3 when phosphorylated

at the corresponding residues. It has been validated in Human, Mouse, Rat, Hamster Monkey, D. melanogaster, Zebrafish and Bovine. Cited in more than 9000 publications. https://www.cellsignal.com/products/primary-antibodies/phospho-akt-ser473-d9e-xp-rabbit-mab/4060?site-search-type=Products&N=4294956287&Ntt=phospho-akt&fromPage=plp

Anti-Akt (pan, Clone 11E7) Rabbit monoclonal antibody (Cell Signaling Technology, Cat #4685): detects endogenous levels of total Akt protein. This antibody does not cross-react with other related proteins. It has been validated in Human, Mouse, Rat and Monkey. Cited in more than 1600 publications. https://www.cellsignal.com/products/primary-antibodies/akt-pan-11e7-rabbit-mab/4685?site-search-type=Products&N=4294956287&Ntt=4685s&fromPage=plp&_requestid=2752015

Anti-α-Tubulin (11H10) Rabbit monoclonal antibody (Cell Signaling Technology, Cat #2125S): This antibody detects endogenous levels of total α-tubulin protein, and does not cross-react with recombinant β-tubulin. It has been validated in Human, Mouse, Rat, Monkey, D. melanogaster, Zebrafish, Bovine, Pig. Cited in more than 650 publications. https://www.cellsignal.com/products/primary-antibodies/a-tubulin-11h10-rabbit-mab/2125?site-search-type=Products&N=4294956287&Ntt=2125s&fromPage=plp&_requestid=1974397

Anti-Zap-70 (99F2) Rabbit monoclonal antibody (Cell Signaling Technology, Cat #2705): This antibody detects endogenous levels of total Zap-70. It has been validated in Human and Mouse Cited in more than 60 publications. https://www.cellsignal.com/products/primary-antibodies/zap-70-99f2-rabbit-mab/2705?site-search-type=Products&N=4294956287&Ntt=2705s&fromPage=plp&_requestid=1975150

Anti-β-Actin (13E5) Rabbit monoclonal antibody (Cell Signaling Technology, Cat #4970): This antibody detects endogenous levels of total β-actin protein. Depsite the high sequence identity between the cytoplasmic actin isoforms, β-actin and cytoplasmic γ-actin, β-Actin (13E5) Rabbit mAb #4970 does not cross-react with cytoplasmic γ-actin, or any other actin isoforms. It has been validated in Human, Mouse, Rat, Monkey, Bovine and Pig. Cited in more than 5000 publications. https://www.cellsignal.com/products/primary-antibodies/b-actin-13e5-rabbit-mab/4970

Anti-PIS1 Antibody (C-2) Mouse monoclonal antibody (Santa Cruz, Cat #sc-514255). This antibody detects PIS-1 (CDIPT) and has been validated in Mouse, Rat and Human. Cited in 2 publications. https://www.scbt.com/p/pis1-antibody-c-2

All flow cytometry antibodies from Biolegend and eBioscience were subjected to standard procedures for flow cytometry validation by the manufacturers. All newly developed clones at BioLegend undergo validation testing for multiple applications. This serves as a cross-check for specificity and provides clarity for research uses. Typically, antibodies are tested by two or more of the below methods (flow cytometry, western blot, chromatin immunoprecipitation, immunofluorescence, immunohistochemistry, biofunctional assays). Thus, the clone cross-validates itself, by demonstrating functionality across orthogonal testing methods. Additionally, the biological induction of the expression further validates the specificity of the antibody. Knockout or knockdown of gene expression, such as with siRNA, is also an excellent tool for target validation.
More information regarding validation and reproducibility can be found online on the manufacturer's website: https://www.biolegend.com/en-us/reproducibility

Eukaryotic cell lines

Policy information about cell lines

Cell line source(s)	The murine E.G7 lymphoblast cell line expressing OVA (EL4-OVA) was purchased from the American Type Culture Collection (ATCC, CRL-2113; RRID: CVCL_3505). The murine melanoma cell line B16-F10-OVA was a kind gift from D. Zehn (parental cell line B16-F10 from ATCC, CRL-6475). The human T lymphocyte cell Jurkat (ATCC, TIB-152) was a kind gift from Jonathan Powell. The BL21 cell line was purchased from Scientific laboratory supplies-reagents (CMC0014) and the Sf9 insect cells were purchased from Thermo Fisher (B82501).
Authentication	No authentication of cell lines was performed.
Mycoplasma contamination	The cell lines were not tested for mycoplasma infections.
Commonly misidentified lines (See ICLAC register)	No commonly misidentified lines were used in this study.

Animals and other organisms

Policy information about studies involving animals; ARRIVE guidelines recommended for reporting animal research

Laboratory animals	C57BL/6J mice (RRID: IMSR_JAX:000664), major histocompatibility complex (MHC) class I-restricted ovalbumin (OVA)-specific TCR OT-I transgenic mice (RRID: IMSR_JAX:003831), CD45.1 congenic mice (RRID: IMSR_JAX:002014) were purchased from The Jackson Laboratory. Male and female mice (8-12 weeks old, age- and sex-matched between experimental conditions) were used. All mice were maintained in the animal facilities at the Max Planck Institute for Immunobiology and Epigenetics or at the Johns Hopkins University under specific-pathogen free (SPF) conditions and following institutional animal use and care guidelines. Mice were exposed to a 14h/10h light/dark cycle and fed ad libitum (Ssniff, V1185-300 or Envigo 2018SX) with acidified water (pH 2.5-3.3). The room temperature and humidity were maintained and monitored.
Wild animals	No wild animals were used.
Field-collected samples	No field-collected animals were used.

Ethics oversight	Euthanasia and animal procedures were conducted on 8-12 weeks old male and/or female mice, age-matched and sex-matched. The animal protocols were approved by the Federal Ministry for Nature, Environment and Consumer Protection of the state of Baden-Württemberg, Germany and by the Johns Hopkins University Animal Care and Use (G16-129, G-17-71 and MO19M71, MO22M15).

Note that full information on the approval of the study protocol must also be provided in the manuscript.

Human research participants

Policy information about studies involving human research participants

Population characteristics	Healthy donor population, patients with an acute EBV infection, patients with melanoma undergoing checkpoint inhibitor therapy. For the healthy donor population and patients with an acute EBV infection, no demographic data were collected. For the melanoma studies, a total of 13 participants was recruited. The median age was 55 years (range 46-90 years. Four patients (31%) were female and 9 patients (69%) were male.
Recruitment	For the healthy donor group, buffy coats were kindly provided by the Institute for Transfusion Medicine and Gene Therapy, Medical Center – University of Freiburg (donor consent, anonymized). Patients (n=3,) with an acute EBV infection were recruited based on clinical symptoms and positivity for EBV-VCA-IgM. All participants gave informed consent. No other selection criteria were used for selecting these patients. Patients (n=13) for the melanoma study were selected based on the following criteria: age > 18 years, histologically confirmed malignant melanoma stage III or IV, no previous treatment with an immune checkpoint inhibitor. Patients with a previously diagnosed immunodeficiency syndrome were excluded. Study participants gave their written informed consent prior to the collection of the first sample. All patients who fulfilled the inclusion criteria and presented for initiation of checkpoint inhibitor treatment at our center were offered the opportunity to participate in the study.
Ethics oversight	Institutional Review Boards (Ethics Committee of the Albert Ludwigs University, Freiburg; #282/11 and #310/18). The study was performed in agreement with the principles expressed in the Declaration of Helsinki (2013). No compensation was offered to human participants.

Note that full information on the approval of the study protocol must also be provided in the manuscript.

Flow Cytometry

Plots

Confirm that:

☒ The axis labels state the marker and fluorochrome used (e.g. CD4-FITC).

☒ The axis scales are clearly visible. Include numbers along axes only for bottom left plot of group (a 'group' is an analysis of identical markers).

☒ All plots are contour plots with outliers or pseudocolor plots.

☒ A numerical value for number of cells or percentage (with statistics) is provided.

Methodology

Sample preparation	To isolate cells from the spleen and lymph nodes of mice, the organs were mashed on a 70 µm strainer in medium containing RPMI1640, 10% heat-inactivated fetal calf serum (FCS), 4 mM glutamine, 1% penicillin/streptomycin solution and 55 µM β-mercaptoethanol. Cell suspensions were treated with Gey's solution for 5 minutes if red blood cell lysis was required. Finally, cells were extensively washed and suspensions used for downstream applications. Purification of CD8+ T cells for cell culture was performed using a mouse CD8+ T cell isolation kit (Stem Cell Technologies, Cat# 19753), following the manufacturer's instructions. To isolate human PBMCs from fresh blood samples, blood was first diluted 1:1 with PBS 1X + 2% FCS. Samples were then layered in SepMateTM PBMC isolation tubes (Stem Cell Technologies) preloaded with Lymphoprep (Stem Cell Technologies) and centrifuged for 10 minutes, at room temperature, 1200 g. The PBMC layer was collected and extensively washed in PBS 1X + 2% FCS and suspensions used for downstream applications. Purification of CD8+ T cells for cell culture was performed using a human CD8+ T cell isolation kit (Stem Cell Technologies, Cat# 17953), following the manufacturer's instructions. Isolation of tumor-infiltrating lymphocytes was performed as follows: mice were humanely euthanized and the tumors were excised. Tumors were chopped in small pieces and digested by shaking at 37°C with 1 mg/ml collagenase IA (Sigma, Cat# C9891) and 50 µg/ml DNAseI (Roche, Cat# 10104159001) for 1h. Digested tumors were passed through a 70 µm filter then the lymphocyte fraction was obtained using a Percoll gradient. CD8+ T cells were isolated by positive selection using CD8 TIL MicroBeads (Miltenyl Biotec, Cat# 130-116-478) according to the manufacturer's instructions. Cell viability was quantified by flow cytometry using LIVE/DEAD TM blue, aqua or near-IR dyes (Invitrogen), following manufacturer instructions. Surface antibody staining was performed in PBS 1X + 2% FCS + 5 mM EDTA, for 30 minutes, at 4C, in the dark. The following antibodies were used for surface staining of murine cells: anti-CD8α (clone 53-6.7, Biolegend Cat #100706, 100712, 100713, 100714, 100738), anti-CD45.1 (clone A20, eBioscience Cat#25-0453-82), anti-CD45.2 (clone 104, BD Cat#553772), anti-CD127 (clone A7R34, Biolegend Cat#135020), anti-KLRG1 (clone MAFA, Biolegend Cat#138418), anti-CD44 (clone IM7, Biolegend Cat#103027, 103056), anti-CD62L (clone MEL-14, Biolegend Cat#104407, 104438), anti-CD25 (clone 3C7, Biolegend Cat#101907 and clone PC61, Biolegend Cat#102008), anti-

PD-1 (clone RMP1-30, Biolegend Cat#109110 and clone 29F.1A12, Biolegend Cat#109110), and anti-CD69 (clone H1.2F3, Biolegend Cat#104512).
The following antibodies were used for surface staining of human cells: anti-CD4-APC-Cy7 (clone RPA-T4, Biolegend Cat#300518), anti-CD8-KrO (clone B9.11, Beckman Coulter Cat#B00067), anti-HLA-DR (clone G46-6, eBioscience Cat#556643).
For intracellular cytokine staining, cells were reactivated with PMA (50 ng/ml; Sigma) and ionomycin (500 ng/ml; Sigma) in the presence of brefeldin A (0.1%; Biolegend) for 5 h before fixation using Cytofix Cytoperm (BD Bioscience) and permeabilization according to the manufacturer's instructions. For analysis of phosphorylated proteins, fixation and permeabilization were performed using the Phosphoflow Fix Buffer I (BD Bioscience), followed by permeabilization with Phosphoflow Perm/Wash Buffer I (BD Bioscience). Intracellular antibodies were added to the cell suspension for 45 min at room temperature. The following antibodies were used for intracellular staining of murine cells: anti-IFNg (clone XMG1.2, Biolegend Cat#505808, 505810 and 505806), anti-Granzyme B (clone GB11, Biolegend Cat#515406 and clone NZGB, eBioscience Cat#12-8898-82), anti-phospho-PLCg1 (clone A17025A, Biolegend Cat#612403), anti-phospho-ERK1/2 (clone 6B8B69, Biolegend Cat#369506), anti-phospho-MEK1 (clone A16117B, Biolegend Cat#610608).
The following antibodies were used for intracellular staining of human cells: anti-Ki67 (clone MIB-1, Agilent Dako Cat#F726801-8).

Cell Trace Violet staining (Thermo Fisher Scientific, #34557) was performed according to the manufacturer's instructions. EdU incorporation was measured using the Click-iT EdU Alexa Fluor 647 Flow Cytometry Assay kit according to the provided instructions (Thermo Fisher Scientific, #C10424).

For analysis of membrane lipid order, cultured effector T cells or Jurkat T cells were first stained with the LIVE/DEAD Fixable Dead Cell Stain Kit (Thermo Fisher Scientific), followed by incubation with 5 µM di-4-ANEPPDHQ (Thermo Fisher Scientific, #D36802) for 30 min in the dark at 37℃, 5% CO2. Flow cytometry analysis was performed on a FACSymphony flow cytometer (BD Bioscience) immediately without washing or fixing the cells. High-order cells emit at ~570 nm, and low-order cells emit at ~630 nm, allowing the gating of two separate populations.

Lipid rafts were quantified by measuring fluorescently labeled cholera toxin b subunit (CTB) which binds to glycosphingolipid GM1, an abundant component of lipid rafts. Cultured TE cells or Jurkat T cells were first stained with the LIVE/DEAD Fixable Dead Cell Stain Kit (Thermo Fisher Scientific), followed by incubation with 25 µg/ml Alexa Fluor 488-conjugated recombinant Cholera Toxin Subunit B (Thermo Fisher Scientific, #C34775) for 30 min in the dark at 4℃. Cells were washed twice with staining buffer prior to flow cytometry acquisition.

Phalloidin staining was performed on fixed and permeabilized cells by incubation with phalloidin (Thermo Fisher Scientific, A22287) at a dilution of 1:200 for 30 min.

Instrument	Cells were acquired on LSRFortessa flow cytometer, FACSCelesta flow cytometer, FACSymphony flow cytometer (BD Bioscience) or CytoFLEX platform (Beckmann Coulter).
Software	Raw data were analyzed with FlowJo (V10.7.2, BD Bioscience).
Cell population abundance	No cell sorting was performed in this study.
Gating strategy	To analyze the CD8+ T cell phenotype, we first selected single cells, then excluded dead cells based on a Live/Dead Fixable Dye staining. CD8+ T cells were selected, and the expression of cell surface or intracellular markers, or the incorporation of EdU, Cell Trace Violet, Cholera Toxin subunit B or staining with di-4-ANEPPDHQ was assessed. In killing assays, EL4-OVA cells were stained with Cell Trace Violet which was used to identify them in a mixed suspension with CD8+ T cells. Viability of these cells was determined based on a Live/Dead Fixable Dye staining.

☒ Tick this box to confirm that a figure exemplifying the gating strategy is provided in the Supplementary Information.